Korean J. Chem. Eng., 37(11), 2020-2040 (2020)
DOI: 10.1007/s11814-020-0598-y

pISSN: 0256-1115
eISSN: 1975-7220

Experimental and modeling study of CO_2 separation by modified Pebax 1657 TFC membranes

Abolfazl Jomekian*, Bahamin Bazooyar, and Reza Mosayebi Behbahani***,†**

*Esfarayen University of Technology, Esfarayen, North Khorasan, Iran
**Department of Design and Engineering, School of Creative Arts and Engineering, Staffordshire University, Stoke-on-Trent, ST4 2DE, United Kingdom
***Gas Engineering Department, Ahvaz Faculty of Petroleum Engineering, Petroleum University of Technology (PUT), Ahvaz, Iran
(*Received 4 April 2020 • Revised 26 May 2020 • Accepted 31 May 2020*)

Abstract−Ionic liquid modified Pebax 1657 thin-film composite (TFC) membranes were synthesized on different porous supports for improved separation of CO_2 from CH_4 and N_2. XRD, SEM, FTIR, TGA, DFT, and BJH tests were utilized for the characterization of TFC membranes and supports. The incorporation of 1,3-Di-n-butyl-2-methylimidazolium chloride ionic liquid into the Pebax 1657 solution led to better compatibility between selective layer and support. The results of gas permeation tests showed an enhanced CO_2/CH_4 and CO_2/N_2 selectivity for most of the ionic liquid modified TFC membranes. To derive a predictive model for the permeability of gases in TFC membranes, correction factors (β) for fractional free volumes of TFC membranes were linearly correlated against correction factors (α) for porosity and tortuosity of the substrate in the dusty gas model using CO_2 experimental permeance data at 20, 60, 100 and 140 °C. The resulting modified model showed remarkable effectiveness in the prediction of permeability of CH_4 and N_2 in the TFC membrane at investigated temperatures. The comparison of model predictive performance with previous models showed the supremacy of the new model in terms of average absolute relative errors (AARE) and the standard deviation of relative errors (σ).

Keywords: TFC Membranes, Ionic Liquid, Pebax 1657, Permeability Prediction, Model

INTRODUCTION

CO_2 is the reason for many industrial and environmental problems. In the natural gas industry, problems such as heat value reduction, pipeline corrosion, hydrate formation, and pressure drop in transmission exist because of the presence of CO_2 in pipelines [1-3]. The release of massive amounts of CO_2 in the atmosphere is considered to be the main reason for global warming and air pollution [4,5]. Although the conventional CO_2 capture methods such as amine-based absorption [6] or cryogenic processes [7] are effective in CO_2 capture from natural gas or gaseous effluents, these methods are known to be energy-intensive processes. Thus, with the current increasing rate of the world's energy demand, there is a need for an alternative process for CO_2 capture. Membrane processes have emerged as one of the more promising methods of CO_2 separation due to its high energy efficiency and ease of operation [8]. Accordingly, studies on the different polymeric, inorganic, mixed matrix, and composite membranes for CO_2 separation have increased extensively, especially in the last two decades. Thin-film composite (TFC) membranes having a thin selective top-layer and a thick porous sub-layer, showed promise in CO_2 separation [9,10]. The pressure normalized flux of a gas in a membrane depends on the thickness of the selective layer as well as its intrinsic permeability. Hence, the reduction of the thickness of the selective layer while maintaining its integrity is one of the most effective approaches to improving the permeation flux of membranes. TFC membranes can be prepared with a thinner selective layer compared to conventional composite membranes; hence, comparably these membranes can provide higher fluxes without a considerable drop in their selective separation performance. The selection of material for selective top-layer and support sub-layer is very important in TFC membrane synthesis. Poly(ether-block-amide) 1657 copolymer with the trade name of Pebax® 1657, which consists of PEO as polyether and nylon 6 as polyamide, showed remarkable performance in CO_2 separation and was used extensively as selective layer material in composite membranes [9,11]. Several studies for improvement of separation performance of Pebax-based conventional, composite, and mixed matrix membranes have been reported, focused on the different types of modification of these membranes in recent years [9,12-15]. Utilization of ionic liquid in modification and functionalization of polymers and copolymers such as Pebax for improvement of the separation performance and compatibility enhancement at the polymer-particle interface in membranes was one of the effective approaches [11,13,15-17]. Fam et al. [9] reported the modification of Pebax 1657 with the introduction of [emim][BF_4] to enhance the CO_2 separation performance of membranes. Bernardo et al. [18] synthesized and examined an ion-gel membrane using an imidazolium-based IL and Pebax 1657 to boost the CO_2 capture.

†To whom correspondence should be addressed.
E-mail: behbahani@put.ac.ir

Rabiee et al. [19] successfully introduced an imidazolium-based IL in Pebax 1657 solution for improvement of CO_2/H_2 selectivity of resulted membranes. These studies on the utilization of imidazolium-based ILs in the Pebax solution showed promising results in CO_2 separation.

It is desired that the substrate of TFC membranes shows proper mechanical stability without affecting the separation performance of the membrane; however, efforts to enhance the mechanical strength of support often lead to the reduction of gas flux. This restriction effect has been studied by several groups in recent years [20-23].

Ramon et al. [22] theoretically studied the effect of pore size and distribution of support on the diffusion of gases through composite membranes. They showed that there is a relationship between flux and support characteristics such as pore size and porosity. Orogbemi et al. [24,25] investigated the effect of synthesized microporous layers with different carbon loadings on gas permeability of the diffusion layer. They showed that the loading of carbon in the support layer directly affected the gas permeability of the whole membrane. Zhu et al. [26] investigated the restriction effect of support on permeation by using polyethersulfone (PES) as the support of different selective layers. They concluded that microporous support causes a significant drop in the efficiency of the TFC separation performance of membranes. Ghadimi et al. [20] investigated the effect of PES microporous supports synthesized by different solvents on the permeation properties of Pebax 1657/PES TFC membranes. They showed that the different geometries of microporous support caused by the incorporation of different solvent in PES have significant and disparate effects on the permeation decline of TFC membranes.

Despite the efforts of various groups to model the gas permeation through TFC membranes, there is a lack of a general relationship between permeation in different porous support types and permeation in TFC membranes. In this work, to improve the predictability of permeation models in TFC membranes based on their support type and porosity, several supports with different pore structures and the regime have been synthesized or prepared and the permeation of CO_2 at different temperatures have been measured in both bare support and TFC membrane. A modified dusty gas model (DGM) for CO_2 permeation in support and a modified model based on Jia and Xu [27] work for CO_2 permeation in TFC membranes have been proposed. The relationship obtained for correction parameters at different temperatures in both models was used for the prediction of CH_4 and N_2 permeabilities in TFC membranes based on the permeation data of porous supports.

In the experimental section of the work, Pebax 1657 was used for the fabrication of a selective layer. The 3-Di-n-butyl-2-methylimidazolium chloride (DnBMCl), an imidazolium-based ionic liquid was prepared and used to enhance the compatibility and interaction between selective top layer and substrate. Two types of support, one based on modified ZIF-8 and the other based on macroporous polycarbonate (PC) were synthesized. The results of CO_2, CH_4, and N_2 permeation tests of TFC membranes with two different types of support were compared with those of a single layer Pebax 1657 membranes and a grindstone-supported Pebax 1657 layers.

The result of this work can be used for estimation of gas permeability of TFC membranes based on permeation data of their support and permeation data of pure single layer membrane synthesized by the same material used for selective layer preparation. This advantage can help researchers be informed about the permeation properties (permeability & selectivity) of their TFC membrane before the start of the synthesis procedure of composite membranes. Since the permeation data for conventional substrates with known pore structure and single-layer polymeric membranes are numerously reported in the literature, using the model presented in this work can save a considerable amount of time, effort, and money for membrane researchers intending to start a gas separation project using TFC membranes.

EXPERIMENTAL

1. Materials

Pebax 1657 was supplied by Arkema Inc. The macroporous PC membrane was supplied by NIPC inc. Phenylenediamine (99%, MPD), Triethylamine (99%, TEA), Acetonitrile (99.8%, ACN), and Sodium Hydroxide (99.8%, NaOH) were purchased from Guangzhou Sinosource Inc. Zinc nitrate hexahydrate (99%, $Zn(NO_3)_2 \cdot 6H_2O$), 2-methyl Imidazole (99%, MeIM), Methanol (99.99% MeOH), Ethanol (99.99%, EtOH), n-Butanol (99.99%, n-BuOH), Sulfuric Acid (99.99%, H_2SO_4), Hydrochloric Acid (99.99%, HCl), (N,N-Dimethylformamide (99.99%, DMF), N-Methyl-2-pyrrolidone (99.99%, NMP), Deionized Water (H_2O) and Normal-Hexane (99.99%, n-hexane) and Methyl dodecylbenzene sulfonate (98%, MDBS), were all purchased from Merck Inc.

2. Synthesis of 1,3-Di-n-butyl-2-methylimidazolium Chloride Ionic Liquid

The preparation procedure of 1,3-Di-n-butyl-2-methylimidazolium chloride (DnBMCl) is similar to the procedure reported in our previous work [11] but with slight modifications in quantities of the precursors used: First, 1-chlorobutanol was synthesized from 17.5 ml of n-Butanol and 20 ml of HCl in the presence of 0.2 ml of H_2SO_4 under reflux for 6 h at 100 °C. The resulting mixture of 1-chlorobutanol and H_2O was physically separated using a centrifuge. In the second step, 2.5 g of 2-methylimidazole and 1.5 g of NaOH were dissolved in 25 ml of ACN and stirred for 1 h, then 1-chlorobutanol was added dropwise to ACN solution at room temperature. An extra hour of stirring resulted in the formation of 1-butyl-2-methylimidazole. In the last step, 1-chlorobutanol was added to the as-synthesized 1-butyl-2-methylimidazole solution and the resulting solution was stirred and heated at 100 °C for 6 h, then batch distillation at 82 °C was applied to remove the solvent from as-synthesized 1,3-Di-n-butyl-2-methylimidazolium chloride.

3. Synthesis of Modified ZIF-8 Porous Support

To synthesize ZIF-8 support, initially, a rigid flat disk of PTFE was used as a seeding surface. The PTFE disk was placed on the bottom of a cylindrical Teflon container and the first precursor solution containing 70 ml of ethanol, 30 ml of water, 2 g of Pebax 1657 granules and 1 g of zinc nitrate hexahydrate ($Zn(NO_3)_2 \cdot 6(H_2O)$) was stirred in a container. The vigorous stirring continued until all the granules of Pebax 1657 completely dissolved. The second precursor solution was prepared by dissolving 13.8 g of 2-methyl Imid-

Table 1. The abbreviated names of different synthesized membranes

Abbreviated names of membranes	Modified/Unmodified with ionic liquid (DnBMCl)	Type of substrate
P*	Unmodified	Without substrate
IP**	Modified	Without substrate
Pgs	Unmodified	Grindstone
IPgs	Modified	Grindstone
PZIF	Unmodified	Modified ZIF-8
IPZIF	Modified	Modified ZIF-8
PmPC	Unmodified	Modified macroporous PC fiber
IPmPC	Modified	Modified macroporous PC fiber

*P: Pebax 1657, **IP: Ionic liquid modified Pebax 1657

azole (MeIM) in 100 ml of 70 vol%-30 vol% of the ethanol-water solution. This prepared solution was poured dropwise for the duration of 6 h on the first precursor solution along with gentle stirring. The container was placed in steel autoclave and the autoclave was placed in an oven for four complete days at 150 °C, boosting the assembly reaction of ZIF-8 particle formation and pore structure modification [28]. After the completion of the assembly reaction, the whole process was halted and the PTFE disk with a grown layer of ZIF-8 on its top was removed from the container bottom. The PTFE disk with ZIF-8 layer on top was subjected to several cycles of washing process under reflux using ethanol as an extractive solvent. After Pebax 1657 removal, the PTFE disk was placed in air for 12 h to dry, then the ZIF-8 layer was separated from the PTFE disk. This layer was ready to be used as a substrate for membranes.

4. Modification of Macroporous PC Support Layer

The macroporous PC support layer was modified based on the approach reported by Calwell and Jackson [29]. A disk shaped part of the macroporous PC was cut and immersed in a 50 ml aqueous solution of 5% m-phenylenediamine and 3% triethylamine and 0.2% Methyl dodecylbenzene sulfonate for 2 h at 30 °C. The saturated PC then was placed on a glass substrate and the excess solution was removed by blowing air at 40 °C parallel to the surface of the PC support for 1 min. The as-modified macroporous PC support layer was then ready to be coated by membrane material.

5. The Preparation of Modified IL-Pebax 1657 Single Layer and TFC Membranes

To modify Pebax 1657 using DnBMCl, initially, a mixture of 4 wt% of Pebax 1657 was prepared by inserting granules of Pebax 1657 in a solution consisting of 40 wt% DnBMCl and 60 wt% methanol. The prepared mixture was then stirred vigorously at 70 °C for 12 h. Afterward, the solution was drained and the remaining Pebax particles were subjected to washing cycles, once by methanol and then twice by ethanol. The resulting material was solid IL-Pebax 1657 particles.

These particles, in the second step, were placed in a solvent consisting of 70 wt% ethanol and 30 wt% water and stirred vigorously at 70 °C for 24 h to yield a 4 wt% IL-Pebax 1657 solution.

The coating method was applied to synthesize IL-Pebax 1657 solution. To do this, a synthesized substrate was kept still at the bottom of the petri dish using tapes. The petri dish had 20 degrees of inclination with the horizon at the time of coating. The prepared solution of IL-Pebax 1657 was poured on the edge of the petri dish gently to cover the whole substrate surface. This procedure was performed three times in four cardinal directions in 2 minutes, which means twelve times of 10 seconds coating for each membrane. For single-layer IL-Pebax 1657 membranes, the whole coating procedure was repeated once again to increase the thickness and mechanical stability of a standalone selective layer. Four similar but unmodified samples were prepared for comparison purposes with the exact as-explained procedure without the part of the introduction of ionic-liquid to the Pebax 1657 solution.

For brevity, the abbreviated names of synthesized samples along with their synthesis characteristics are presented in Table 1.

6. Gas Permeation Measurements

Gas permeation measurements were conducted using a constant pressure-variable volume pre-built setup (Fig. 1). As can be seen in Fig. 2, two types of flat sheet membrane modules were fabricated, a PTFE module, specifically designed for composite membranes permeation tests, and a stainless steel module, fabricated for single-layer membrane permeation tests. The pure and mixed gas experiments were all conducted at 20 °C. Utilizing the permeation setup, binary gas mixtures (with CO_2 as constant and CH_4 or N_2 as replaceable components) were generated to evaluate membranes. The permeation data along with errors for each membrane were recorded from three distinct samples of that membrane which was synthesized exactly by the same procedures.

The permeance of gases in pure gas tests was directly calculated from the gas flux data measured by a bubble flow meter with the well-known defining Eq. (1):

$$P = \frac{Q}{A(p_f - p_p)} \tag{1}$$

where P is permeance coefficient (cm^3(STP)/(s cm^2 cmHg)), Q is the volumetric flowrate (cm^3/s), A is the effective membrane area (cm^2) for gas permeation, and p_f and p_p are pressures at feed and permeate side (cmHg), respectively.

For the binary mixed gas permeation measurements the following equation was applied [14,30]:

$$P_i = \frac{y_i Q}{A(p_f x_i - p_p y_i)} \tag{2}$$

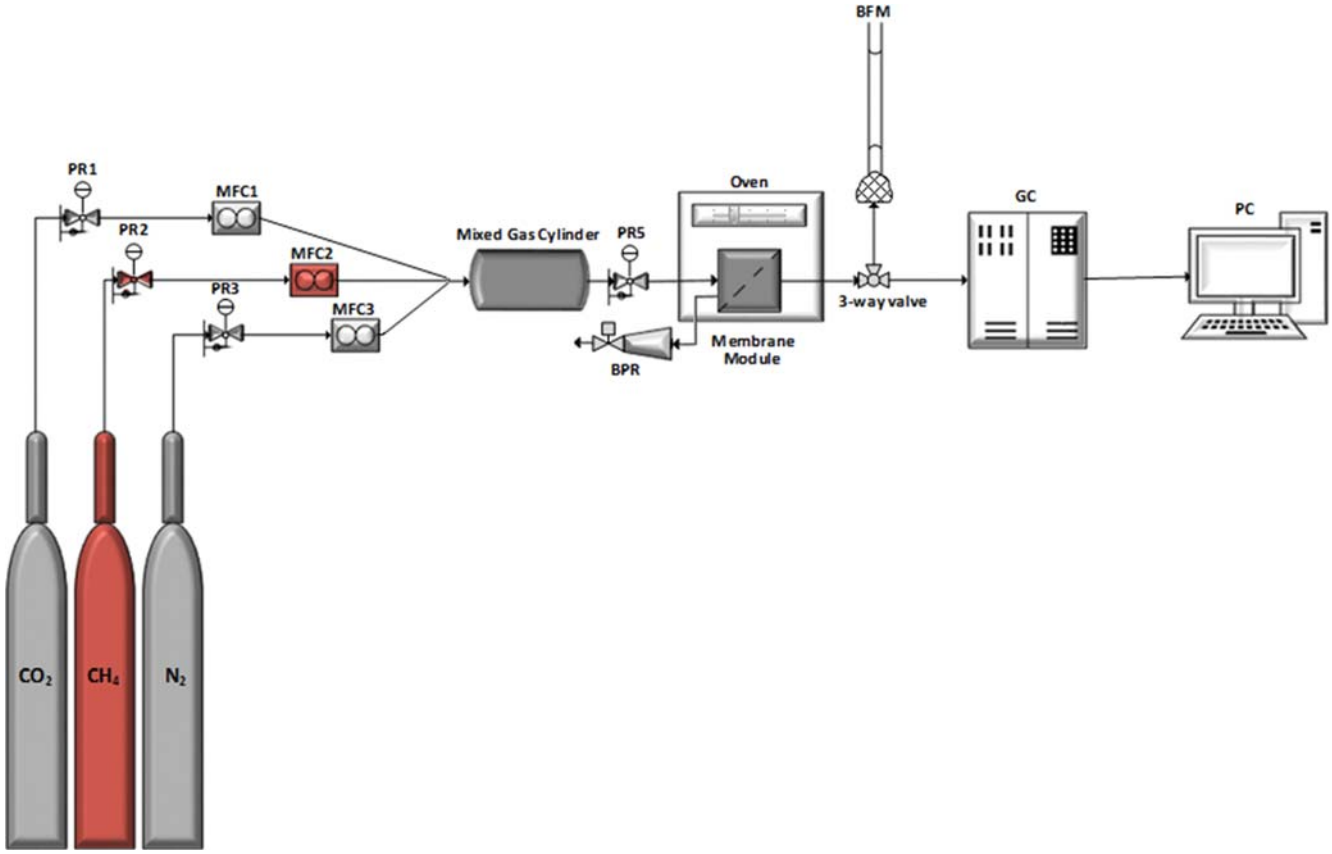

Fig. 1. Schematic diagram of mixed gas permeation test set-up.
PR: Pressure regulator BPR: Back-pressure regulator GC: Gas chromatography
MFC: Mass flow controller BFM: Bubble flow meter PC: Personal computer

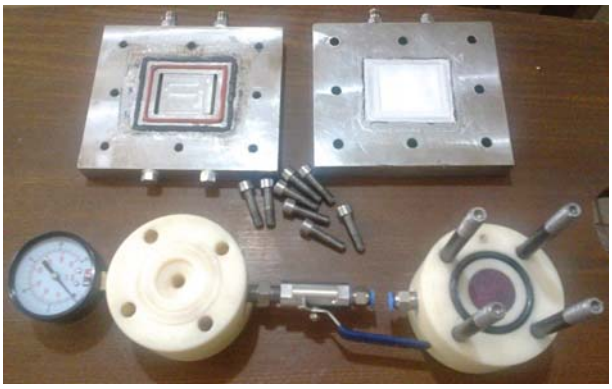

Fig. 2. The fabricated membrane modules for gas permeation experiments.

where P_i is permeance coefficient (cm^3(STP)/(s cm^2 cmHg)) of component i, y_i and x_i are mole fractions of component i in permeate and feed side, respectively.

The selectivity $\alpha_{A/B}$ is defined as the gas permeability ratio of more permeable gas (P_A) to that of the less permeable gas (P_B):

$$\alpha_{A/B}=\frac{P_A}{P_B} \quad (3)$$

For mixed gas permeation tests, two different mixtures of gases were generated using gas permeation setup. The gas compositions of permeate gas streams were analyzed by a gas chromatograph (GC) equipped with thermal conductivity detectors (TCDs) (ACME 6100, Korea).

CHARACTERIZATION

An X-ray diffractometer (XRD-6100, Shimadzu) was used with settings of Cu Ka radiation (30 kV-40 mA) at step time 1 s and step size of 0.1° by scanning 2θ angle between 1° and 60° to determine the formation of ZIF-8 pure phase and to acquire information about the crystallinity degree and crystal size. To visualize the morphology of surface and cross-section of membranes selective layers and supports, scanning electron microscopy (SEM) (FEG-7001 (JEOL)) was applied. To provide insight about the interactions of molecular groups at the interface of support and selective layer, a Fourier transform infrared spectrophotometer (IRAffinity-1S, Shimadzu) with an average of 16 scans in the range of 600-4,000 cm^{-1} was applied. An adsorption instrument (Micrometrics, ASAP 2020) was used to measure the mean pore diameter of porous substrates by DFT and BJH method for modified ZIF-8 and grindstone substrates, respectively. Thermogravimetric analysis was performed using (TGA-50, Shimadzu) with a temperature ramp of

5 °C/min from 25 °C to 600 °C.

For the calculation of fractional free volume (FFV) of membranes, the density of membranes and substrates had to be measured. The densities of membranes and substrates was measured by a method based on the Archimedean principle. A microanalytical balance (BM-22, AND) was utilized to measure the weights of samples and to calculate densities based on the following equation:

$$\rho = \frac{W_{air}}{W_{air} - W_{liq}}(\rho_{liq} - \rho_{air}) + \rho_{air} \quad (4)$$

where W_{air} is the weight of sample in air, W_{liq} represents the measured weight of floating or submerged samples in a liquid with known density (i.e., ethanol, n-hexane, silicon oil, etc.), ρ_{air} and ρ_{liq} are, respectively, the densities of air and selected liquid. In this study, ethanol was used for density measurements.

MODELING OF GAS TRANSPORT

1. Modeling of Gas Transport through the Porous Support

1-1. Viscous Flow

This mechanism of transport is valid for gas transport in macropores. The molar flux (J_v) can be expressed based on a pressure gradient by a Hagen-Poiseuille type equation [21]:

$$J_v = -\frac{\varepsilon}{\tau}\frac{d_p^2}{32}\frac{p}{\mu RT}\frac{dp}{dz} \quad (5)$$

where μ is the gas viscosity, p is the applied pressure, T is the temperature, R is the universal gas constant, and z is the direction of diffusion. The factor ε is the porosity and the factor τ is the tortuosity of passage media. The ε/τ is the combined factor that is introduced in the equation to account for the geometry of the pores in porous media.

Integration of Eq. (4) over the thickness of porous media and dividing by the pressure difference across the media gives the pressure-normalized flux or permeance of penetrant through media at steady state:

$$\Pi_v = \frac{J_v}{\Delta p} = \frac{\varepsilon}{\tau}\frac{d_p^2}{32}\frac{\bar{p}}{\mu RT\delta}\pi \quad (6)$$

where δ is the thickness of porous media, $\bar{p}$ is the arithmetic mean of upstream and downstream pressures.

1-2. Knudsen Diffusion

This mechanism of diffusion is valid for diffusion in mesopores, the pores with mean pore diameters in the range of 2-50 nm. Under this regime the collision of molecules with pore walls is important in diffusion, accordingly, the Knudsen diffusion coefficient is expressed by the following formula [31]:

$$D_{Kn} = \frac{d_p}{3}\left(\frac{8RT}{\pi M}\right)^{0.5} \quad (7)$$

where M is the molecular weight of the penetrating gas. Since not all of the gas molecules in the pores diffuse in the considered direction, a geometric factor of 1/3 is introduced to only account for the molecules moving in the considered direction. The combination of Fick's first law considering the Knudsen diffusion coefficient and the non-ideality of the pore structure gives the gas flux through the pores by [32]:

$$J_K = -\frac{\varepsilon}{\tau RT} D_{Kn}\frac{dp}{dz} \quad (8)$$

The integration of Eq. (8) over the thickness of porous media and dividing by the pressure difference across the media gives the permeance of penetrant through media:

$$\Pi_K = \frac{J_K}{\Delta p} = \frac{\varepsilon}{\tau\delta RT} D_{Kn} \quad (9)$$

1-3. The Modified Dusty Gas Model (DGM)

The combination of viscous flow and Knudsen diffusion into one model leads to a truncated dusty gas model (DGM). This model considers the porous medium as large gas molecules limited by the space. A porous medium with the pore size range of 10-1,000 nm is a valid medium for modeling of gas transport by DGM [33]. Ignoring the continuum diffusion, this model is used to predict the permeance of penetrants in a porous support layer by the following formula [34]:

$$\Pi_{DGM} = \varepsilon\left(\frac{d_p^2}{32\delta_{skin}}\frac{\bar{p}}{\mu RT} + \frac{d_p}{3\delta_{skin}}\left(\frac{8}{\pi MRT}\right)^{0.5}\right) \quad (10)$$

As can be seen, there are minor differences between a combination of viscous flow and Knudsen diffusion with DGM. The ε in DGM is the surface porosity, which involves the correlated tortuosity, and δ_{skin} is the thickness of the top layer of the porous support. The reason for this simplification was because it was assumed that the permeance of the porous substrate is mainly controlled by its thin top-layer and not by the thick porous sub-layer [20]. This is not exactly correct for the supports, which have uniform pore structure and small pore diameter. Therefore, in this work, to account for the gas transport resistance in the porous sub-layer, the following combination of viscous flow and Knudsen diffusion was considered as the fundamental gas transport model in the support layer:

$$\Pi_{V\&K} = \Pi_V + \Pi_K = \frac{\varepsilon}{\tau}\left(\frac{d_p^2}{32\delta\mu}\frac{\bar{p}}{RT} + \frac{d_p}{3\delta}\left(\frac{8}{\pi MRT}\right)^{0.5}\right) \quad (11)$$

where ε/τ is a parameter related to the pore geometry and δ in the thickness of the whole support layer. The ε/τ is the only difficult parameter in Eq. (10) to measure. Several different approaches were applied to estimate ε and τ [26,35]. However, most of them are approximations, considering ε as surface porosity and correlating τ to ε by a simple equation. To avoid such simplifying assumption in this work, as a novel approach ε/τ was replaced by measured void volume (φ_v) of the substrate. This parameter accounts for the porosity of the porous support layer. The void volume (φ_v) of the substrate is calculated by the following formula:

$$\varphi_v = 1 - \frac{\rho_{unit}}{\rho_{bulk}} \quad (12)$$

where ρ_{unit} is the measured density of unit synthetic material and ρ_{bulk} is the measured density of the fabricated substrate.

φ_v was multiplied by a correction factor (α) to account for the tortuosity and isolated pores which cannot be accessed during density measurement experiments. Hence, the modified DGM

model with the following equation was proposed for prediction of permeance of gases in porous media:

$$\Pi_{modified\ DGM} = \alpha\varphi_v\left(\frac{d_p^2}{32\delta\mu RT}\frac{\bar{p}}{RT} + \frac{d_p}{3\delta}\left(\frac{8}{\pi MRT}\right)^{0.5}\right) \quad (13)$$

2. Modeling of Gas Transport through Pebax 1657 TFC Membrane

Jia and Xu [27] have proposed a model verified by over sixty different polymers that predict the permeability of several gases in different polymers. In their model, the permeability of gases in polymers was expressed based on an exponential function of free volume and cohesive energy density by the following formula:

$$\log P = a_1 + b_1\left(\frac{\nu_f}{E_{coh}}\right) \quad (14)$$

where a_1 and b_1 are constants dependent on the penetrating gas, ν_f is the free volume of the membrane and E_{coh} is the cohesive energy density of gas in the polymer.

The parameter ν_f/E_{coh} for different polymers is reported by Jia and Xu for conventional polymers; however, for copolymers, there are rarely reported such data in the literature. Hence, in this work, the following relationship, which is based on the weight percent of PEO and PA6 in the structure of Pebax 1657, was used for estimation of ν_f/E_{coh} of Pebax 1657.

$$\left(\frac{\nu_f}{E_{coh}}\right)_{Pebax1657} = \omega_{PEO}\left(\frac{\nu_f}{E_{coh}}\right)_{PEO} + \omega_{PA6}\left(\frac{\nu_f}{E_{coh}}\right)_{PA6} \quad (15)$$

where ω_{PEO} and ω_{PA6} are weight percent of PEO and PA6 in Pebax 1657 structure which are 0.6 and 0.4 respectively. The permeability of TFC membranes (P_i) was calculated based on measured permeance and the effective thickness of the selective layer ($\delta_{effective}$) by the following formula:

$$P(\text{Barrer}) = \Pi(\text{GPU}) \times \delta_{effective}(\mu m) \quad (16)$$

The effective thickness of the selective layer was estimated using the permeability of standalone single-layer modified and unmodified Pebax 1657 membranes regarding the fact that the Pebax 1657 layer is dense and shows significantly stronger resistance against gas flow compared with porous support.

The fractional free volumes of all synthesized membranes were calculated based on measured densities of membranes and substrates by the Archimedean principle (Eq. (4)). For pristine Pebax 1657 membranes, the FFVs were calculated using the following equation [36,37].

$$FFV = \frac{V_{Pebax} - V_{0,\,Pebax}}{V_{Pebax}} = \frac{M_{Pebax}/\rho_{Pebax} - 1.3V_{W,\,Pebax}}{M_{Pebax}/\rho_{Pebax}} = \frac{\nu_{f,\,Pebax}}{M_{Pebax}/\rho_{Pebax}} \quad (17)$$

where V_{Pebax} is the total molar volume of Pebax 1657 (cm^3mol^{-1}), $V_{0,\,Pebax}$ is the volume occupied by polymer chains (cm^3mol^{-1}), M_{Pebax} is the molar weight of a monomer of Pebax 1657 ($gmol^{-1}$), ρ_{Pebax} is the density of pure Pebax 1657 membrane (gcm^{-3}), and $V_{W,\,Pebax}$ is the van der Waals volume of Pebax 1657 (cm^3mol^{-1}). The van der Waals volume in this study was determined by Bondi's group contribution method by taking into account PEO and PA6 segments in the structure of Pebax 1657. The value of V_W=95.09 cm^3mol^{-1} was obtained for Pebax 1657 [38].

To calculate the FFVs of TFC membranes, both substrate and Pebax 1657 selective layer must be considered. Accordingly, the weight of substrate and TFC membranes after preparation was measured using a microbalance. This provides weight percent of Pebax 1657 and substrate material in the whole TFC membrane. The weight percent of the substrate is used for the calculation of substrate volume fraction according to the following formula [36]:

$$\varphi_{subs} = \frac{\omega_{subs}/\rho_{subs}}{\omega_{subs}/\rho_{subs} + (1-\omega_{subs})/\rho_{Pebax}} \quad (18)$$

where φ_{subs} is the volume fraction of substrate in the TFC membrane, ω_{subs} is the mass fraction of substrate in the TFC membrane, and ρ_{subs} is the density of substrate before it was coated by Pebax 1657 solution.

Using φ_{subs} and ρ_{subs}, the FFVs for TFC membranes can be calculated by the following equation: [8]

$$FFV = \frac{v_{TFC} - [(1.3V_{W,\,Pebax}/M_{Pebax})(1-\varphi_{subs}) + (\varphi_{subs}/\rho_{subs})]}{v_{TFC}} \quad (19)$$

where v_{TFC} is the specific volume of TFC membranes (cm^3g^{-1}) which is the inverse of the density of TFC membranes.

Based on a claim by Thran et al. [39], the Jia and Xu model cannot predict the permeability of some polymers because of the nature of polymers investigated and possible errors in their experimental investigations. We hypothesize that the calculation of FFV based on measured density may encounter some errors due to the ignorance of isolated pores in the structure of the TFC membrane. Hence a modified version of Jia and Xu model has been proposed in this work.

Using calculated FFVs, the following modified equation has been used to predict the permeability of TFC membranes:

$$\log P = a_1 + b_1\left(\frac{\beta \times FFV \times v_{membrane}}{E_{coh}}\right) \quad (20)$$

where $v_{membrane}$ is the molar volume of the single layer or TFC membrane (cm^3mol^{-1}), FFV is the calculated fractional free volume of membrane, and β is a correction factor of FFV which accounts for the isolated pores in the single layer or TFC membrane.

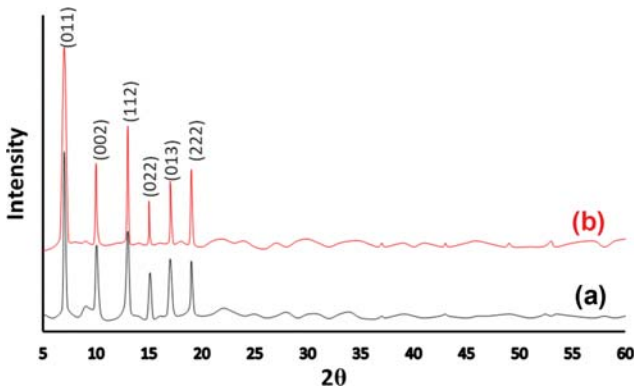

Fig. 3. The XRD pattern of (a) PZIF and (b) IPZIF TFC membrane samples.

RESULTS AND DISCUSSION

1. Results and Discussion of Experimental Part

1-1. XRD Analysis

The XRD patterns related to the (PZIF) and (IPZIF) samples, synthesized on modified ZIF-8 porous support are presented in Fig. 3.

As can be seen in spectra (a) and (b) in this figure, the distinct major peaks from left to right of 2θ axis, which are in respective related to reflection of X-ray from the planes of the crystal structure at coordination of (001), (002), (112), (022), (013) and (222), are the characteristic peaks of ZIF-8 structure [40]. From the com-

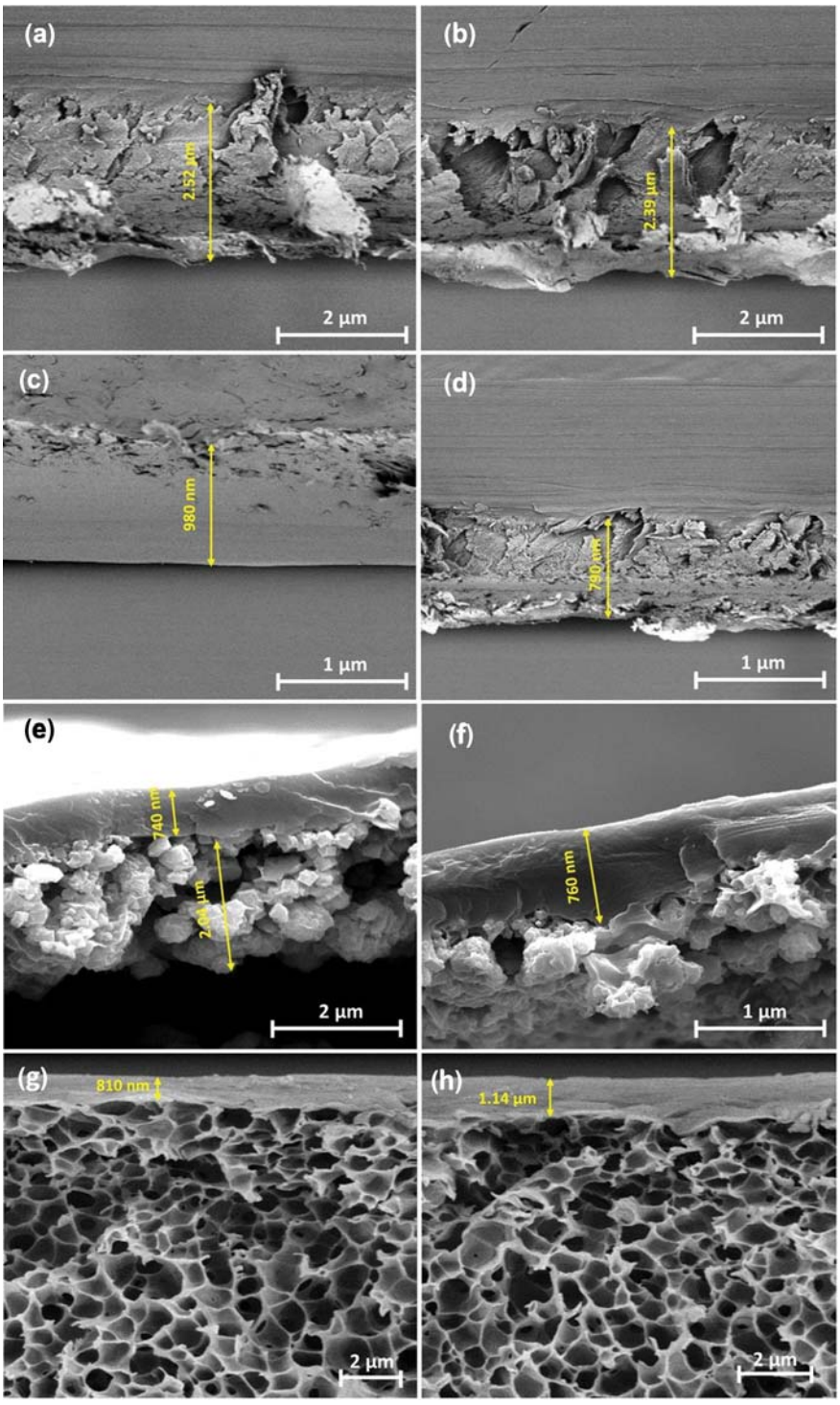

Fig. 4. The SEM micrographs from the cross-sections of (a) P, (b) IP, (c) Pgs, (d) IPgs, (e) PZIF, (f) IPZIF, (g) PmPC and (h) IPmPC membrane samples.

parison of the spectrum of PZIF sample (a) with that of IPZIF sample (b), there are significant similarities in the intensity and position of the main peaks in both spectra. It demonstrates that the pure ZIF-8 particles are fabricated with notable similarities in crystal shape and size. The possible interaction of the selective layer and support did not affect the crystal characteristics in the support layer.

1-2. SEM Analysis

The SEM images from the cross-sections of all synthesized samples are presented in Fig. 4(a)-(h).

As can be seen in Fig. 4(a) and (b), which are respectively related to P and IP samples, the thickness of the selective layer is 2.39-2.52 μm. This range for the thickness of the selective layer is higher than that normally reported for TFC membranes; however, since this is a standalone single layer membrane, fabrication of membrane with higher thickness is necessary to guarantee the required mechanical stability for membrane during permeation experiments at high pressures. Compared to Fig. 4(a) and (b), thinner dense membranes can be observed in Fig. 4(c) and (d) which are related to (Pgs) and (IPgs) samples, respectively. The selective layer thick-

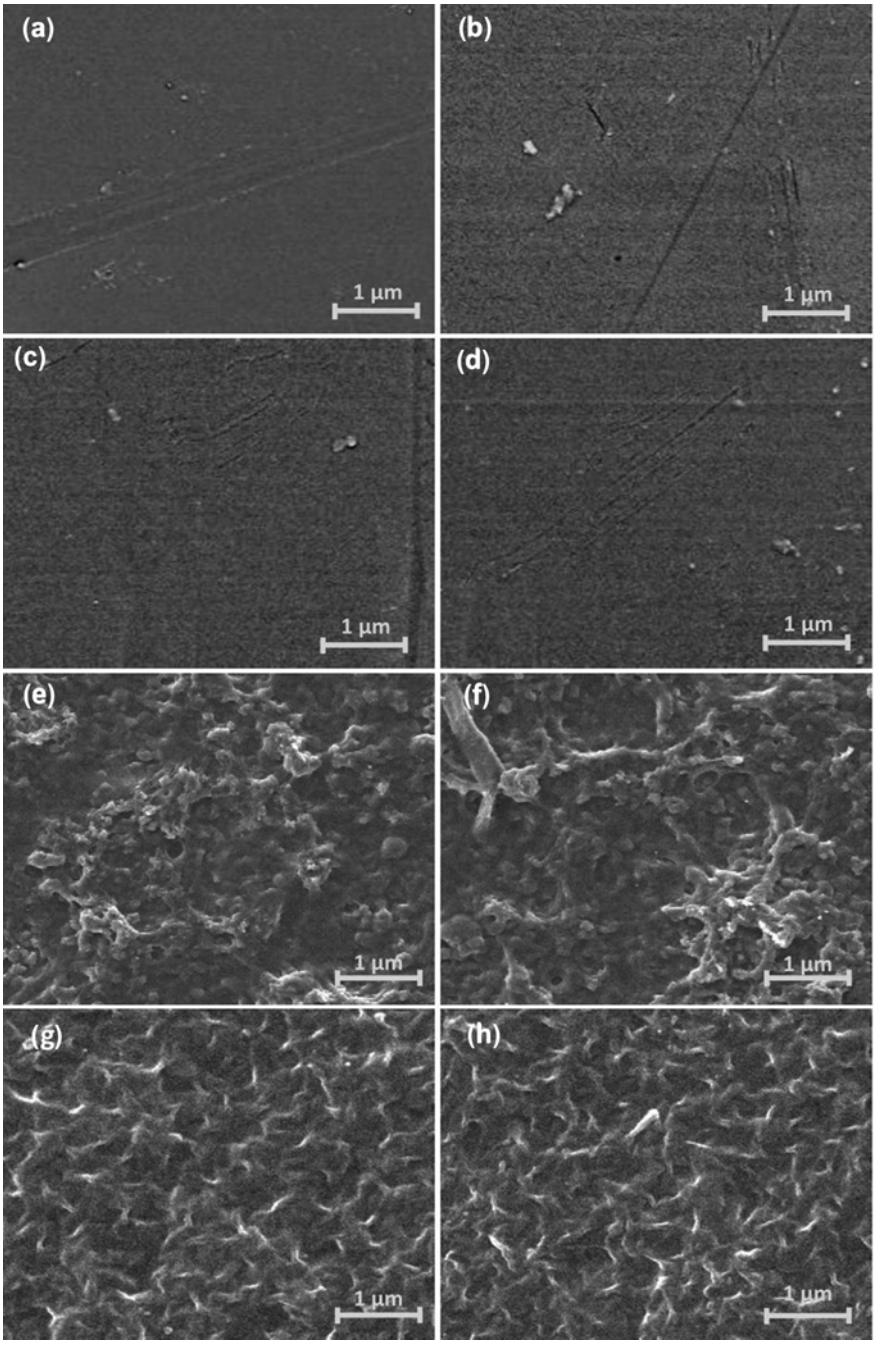

Fig. 5. The SEM micrographs from the surfaces of (a) P, (b) IP, (c) Pgs, (d) IPgs, (e) PZIF, (f) IPZIF, (g) PmPC and (h) IPmPC membrane samples.

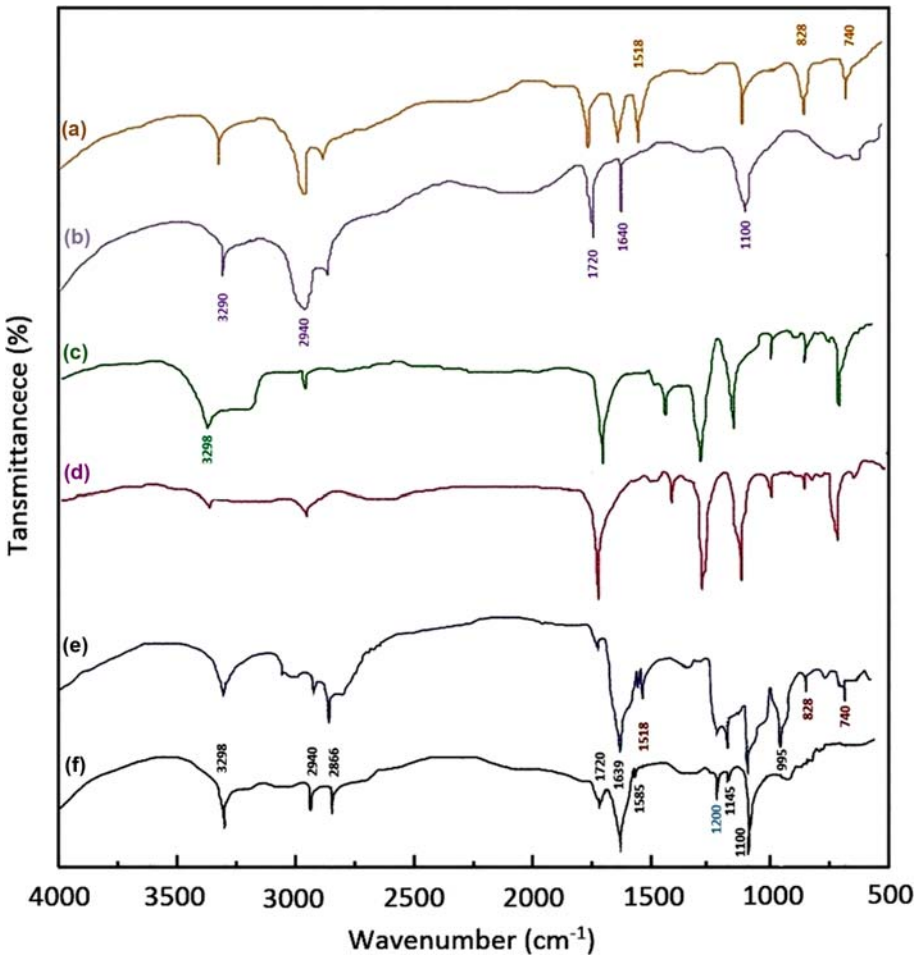

Fig. 6. The FTIR spectra of (a) IP, (b) P, (c) IPmPC, (d) PmPC, (e) IPZIF and (f) PZIF membrane samples.

ness in both samples is about 0.7-1 μm. The cross-sectional images of Fig. 4(e) and (f) demonstrate the integrity of thin selective layers in both modified (IPZIF) and unmodified (PZIF). The thickness of the selective layer is of the same order of magnitude of that of (Pgs) and (IPgs) samples. Considering the roughness of ZIF-8 support layer, which is clear in both micrographs, the lower thickness of the selective layer most probably results in surface defects. The same reason is also valid for (PmPC) and (IPmPC) samples, in which their cross-sectional SEM images are presented in Fig. 4(g) and (h). As can be seen, the coating of Pebax 1657 on enhanced macroporous PC fabric seems to be defect-free; however, there may be a minor intrusion of coating solution into the support.

The integrity of different types of Pebax and IL-Pebax 1657 can be observed in the SEM images of the surface of membranes in Fig. 5. Subfigures (a), (b), (c) and d of Fig. 5, which are related to the synthesized single layer membrane, show noticeable smoothness, while some roughness can be observed on the surfaces of membranes (TFCs) synthesized on ZIF-8 or PC macroporous support (subfigures (e), (f), (g), and (h)). Although in TFC membranes, because of rough support, the selective layer is not as smooth as single-layer membranes, the integrity of the selective layer can be seen without noticeable defect on the surface of membranes. This demonstrates that the coating layer has the appropriate thickness for the fabrication of these types of TFCs.

1-3. FTIR Analysis

The FTIR spectra of all synthesized membranes are presented in Fig. 6(a)-(g).

Spectra (a) and (b) in Fig. 6 are related to samples (IP) and (P), respectively. The characteristic minimums for (P) are at wavenumbers of 1,100, 1,640, 1,720, 2,940, and 3,290 cm^{-1} which respectively are related to stretching vibration of C-O, H-N-C=O group, stretching vibration of C=O, stretching vibration of C-H, and finally N-H group. The observed minimums for Pebax 1657 pristine sample (P) are in good agreement with the IR spectrum of this polymer in Murali et al. [41]. Both a and b spectra are similar except for at the minimums at wavenumbers of 740, 828, and 1,518 cm^{-1}. These belong to out-of-plane C-H bending, bending of in-plane, and C=C bond vibration of the imidazole ring, respectively [11]. This difference in spectra of modified and unmodified Pebax 1657 membranes suggests that DnBMCl is most probably attached to the surface of the Pebax 1657 in (IP) sample. The (c) and (d), IR spectra related to (IPmPC) and (PmPC) samples are very similar except for the intensity of a minimum at 3,298 cm^{-1}; this minimum is related to stretching vibration of N-H which is strong in (IPmPC) and weak in (PmPC) spectra. This is because with the introduction of DnBMCl, an imidazolium-based ionic liquid, due to the

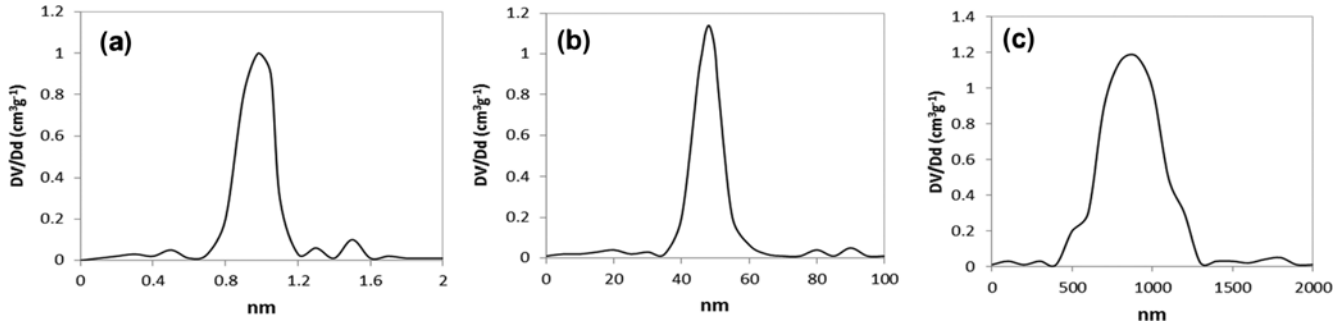

Fig. 7. The pore size distribution of (a) modified ZIF-8, (b) grindstone, and (c) modified macroporous PC substrates.

presence of N-H bonds in the imidazole group, the relative abundance of N-H bonds in whole membrane increases. Therefore, a more intense minimum has been observed in (IPmPC) spectrum.

Despite the differences at wavenumbers of 740, 828, and 1,518 cm^{-1} between spectra (e) and (f), in Fig. 6 which respectively belong to (P-ZIF) and (IP-ZIF) samples, a difference in wavenumber of 1,200 cm^{-1} can also be observed. This minimum is representative of the stretching vibration of the C-C single bond in both samples [42]; however, the minimum of the IR spectrum of (IP-ZIF) is noticeably more clear than that for (P-ZIF). This indicates that the relative abundance of C-C bonds in the IL-modified membrane is higher [42]. Hence, there may be C-C bonds between carbons in the structures of ZIF-8 and carbons in DnBMCl structure.

1-4. Pore Size Distribution (PSD)

The PSD of different utilized substrates is presented in Fig. 7(a)-(c).

As can be seen in this figure, the mean pore size of the modified ZIF-8 substrate is about 1 nm (Fig. 7(a)). This demonstrates that the modified ZIF-8 support has pores in the microporous regime. The relatively narrow peak of pore sizes of modified ZIF-8 indicates the generation of uniform pore sizes during the synthesis procedure. This uniformity in pore size is also observable in Fig. 7(b) which is related to the grindstone. The grindstone shows a mean pore size of about 48 nm, which demonstrates the mesoporosity of this substrate. Fig. 7(c), which is related to macroporous PC substrate, shows a mean pore size of about 894 nm. The PC substrate shows relatively broad pore size distribution, meaning that PC possesses relatively nonuniform pores.

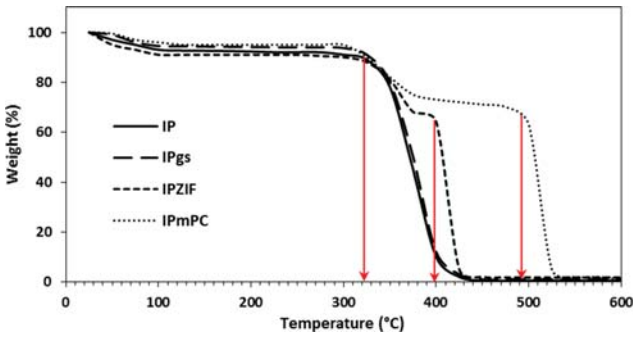

Fig. 8. The thermograms of (IP), (IPgs), (IPZIF), and (IPmPC) membrane samples.

1-5. Thermogravimetric Analysis

The results of TGA of IL-modified samples are presented in Fig. 8.

As expected, the thermograms of (IP) and (IPgs, without grindstone support) samples are very similar and both have two distinct stages of weight loss. The first one, which is below 100 °C, is mainly related to the vaporization of absorbed moisture in samples, and the second one is related to the decomposition of Pebax polymeric structure which occurred at 322 °C. The thermograms of (IPZIF) and (IPmPC) samples, however, show three distinct stages of weight loss. The first and the second of weight loss stages are similar to what was observed for (IP) and (IPgs) samples, but the third stage is due to the decomposition of ZIF-8 at 398 °C for (IPZIF) sample and the degradation of polycarbonate support at 492 °C for (IPmPC) sample. From the results of TGA of IL-modified samples, it can be concluded that all of the samples are thermally stable up to 300 °C; hence, it is expected that no significant change in matrix of membranes occurs during permeation test at temperatures as high as 140 °C.

1-6. Pure Gas Permeation Tests

The CO_2, CH_4, and N_2 permeance of all synthesized membranes

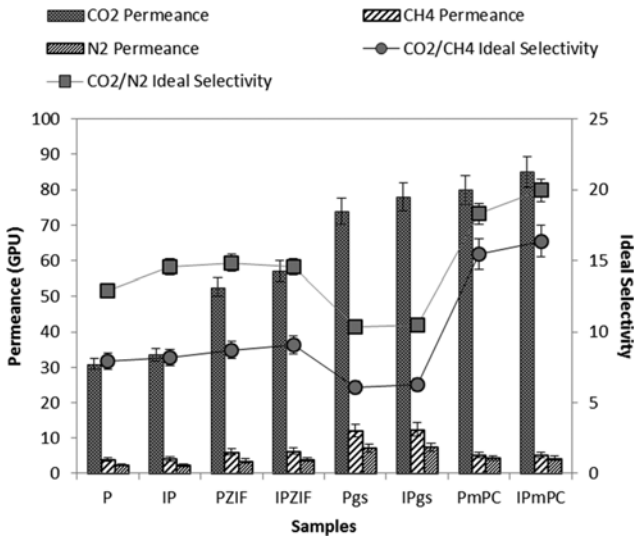

Fig. 9. The pure gas permeance of CO_2, CH_4 and N_2 and ideal selectivity of CO_2/CH_4 and CO_2/N_2 for all synthesized membrane samples at the feed pressure of 4 bars and 20 °C.

along with their CO_2/CH_4 and CO_2/N_2 ideal selectivity are presented in Fig. 9.

As can be seen, the permeance of all TFC membranes is higher than that of IL-modified and unmodified single layer Pebax 1657 membranes. This is mainly because TFC membranes have a significantly thinner selective layer compared with single-layer membranes. The thickness of the selective layer is inversely related to the flux of penetrating gas, hence generally higher gas fluxes are observed for membranes with thinner selective layers. The other noteworthy point in this figure is that besides having high permeance, (PmPC) and (IPmPC) samples show notably higher CO_2/CH_4 and CO_2/N_2 selectivity compared with other synthesized membrane samples. This is most probably related to the macroporous substrate of the TFC membrane. The large pores were partially filled with the coating solution of the Pebax 1657 layer on the surface of the support; hence a more resistible layer could be formed, which causes the diffusion of larger molecules such as N_2 and CH_4 to become more difficult [43,44]. However, for the case of CO_2 permeation, the amine-functionalized support might be the reason for enhanced sorption of CO_2 due to the natural affinity of amine groups at the PC surface for CO_2 [45,46]. This leads to the observation of higher CO_2 permeance in (PmPC) and (IPmPC) samples despite the blockage of some pores. Another noteworthy point extractable from this result is that, generally, the IL modified TFC membranes show higher CO_2/CH_4 and CO_2/N_2 selectivity compared with their corresponding unmodified versions. This is mainly related to the fact that the imidazolium-based ionic liquids have elevated affinity for CO_2 sorption, which is numerously approved in previous investigations. The reason is related to the affinity of the anion group of imidazolium-based ionic liquids for interaction with CO_2 [47]. Among different anions participating in the formation of imidazolium-based ILs, Cl^- is one of the favorite anion groups for CO_2 sorption [48]. Hence DnBMCl modified membrane is expected to have higher sorption affinity for CO_2 and consequently higher CO_2/CH_4 and CO_2/N_2 selectivity compared with unmodified versions of membranes. As was observed in SEM images, the thickness of the selective layer of synthesized membranes in this study was higher than conventional TFC membrane due to the nature of the porous supports used in this work; however, the results of the permeation test are reasonable when compared to the results reported by some reliable previous literature on Pebax 1657 based membranes synthesized with selective layers with different thicknesses [9,13,16,49-51].

The effect of pressure on the separation performance of IL-modified membranes is presented in Fig. 10.

As can be seen in Fig. 10(a), (b), and (c) with the increase in feed pressure the CO_2, CH_4, and N_2 permeances of all IL-modified membranes increase. This change in permeance of all modified membranes with pressure resulted from the combination of the following three main reasons: 1-Partial reduction of the fractional free volume of polymer, 2-Enhanced diffusivity of gases, and 3-Increased sorption of gases in Pebax 1657 matrix. The first reason, which causes the permeation reduction, has a minor effect on permeation through modified Pebax membranes because the

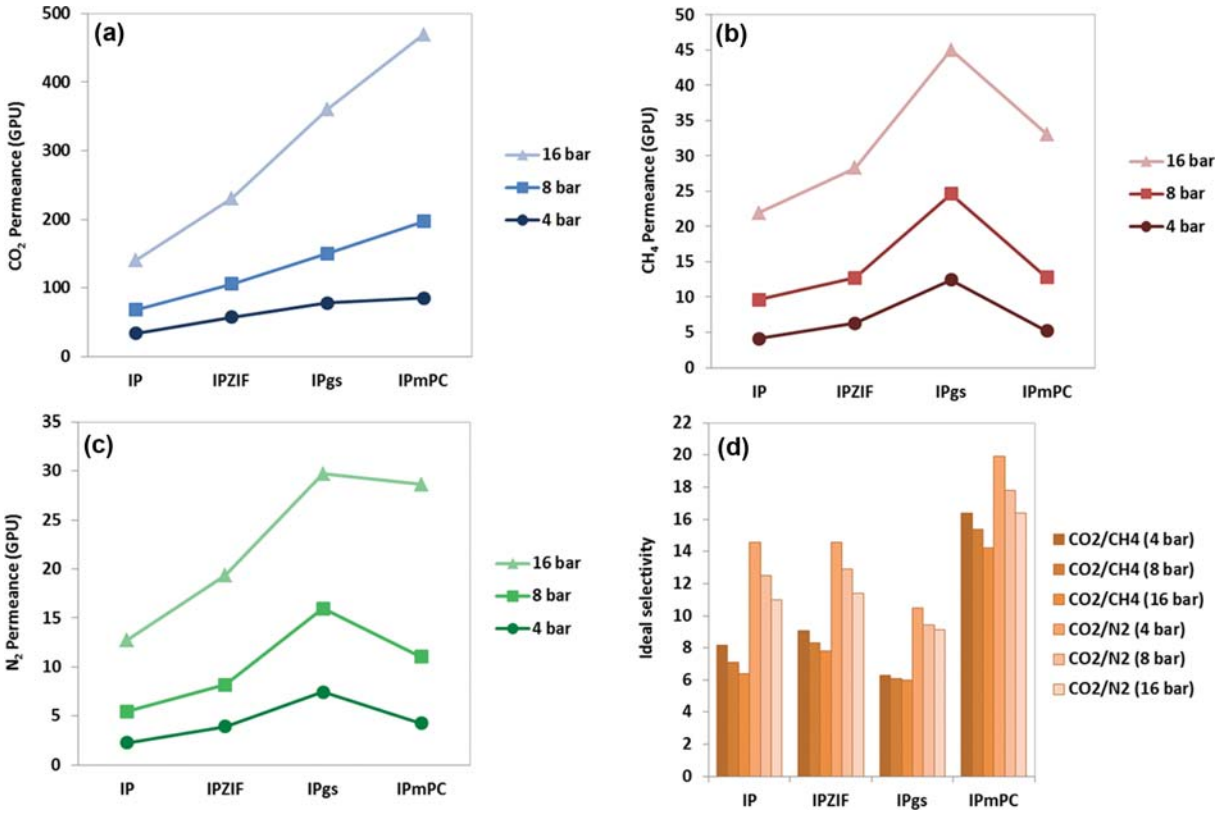

Fig. 10. The changes of (a) CO_2, (b) CH_4, (c) N_2 permeances and (d) CO_2/CH_4 and CO_2/N_2 selectivity with pressure for IL-modified membrane samples.

synthesized membranes are dense with no porosity. However, the second and third reasons have major effects on permeance of membranes since the elevated pressure difference across the membrane has increased the driving force for diffusion and chemical potential for sorption of gases through membranes, leading to the observation of higher permeance and permeability of all investigated gases in IL-Pebax membranes. The increased gas sorption leads to the occurrence of plasticization phenomenon which is often observed in membranes with high affinity for CO_2. This phenomenon, which became more severe in higher pressure, causes local segmental motions in Pebax polymer chains. This alteration in chain packing causes a decline in membrane selectivity, leading to the observation of the increase in fluxes of all investigated gases at high pressures. This was also observed in previous works; however, the effect of plasticization in this work on selectivity is not as severe as what was observed in other reports, including our previous work. This was because the ionic liquid in this work was just used to functionalize the surface of Pebax 1657 and the concentration of ionic liquid used in the matrix of polymer is negligible. Moreover, pure Pebax 1657 polymer was used in this work without the incorporation of CO_2 solubility enhancers such as ZIF-8 and ZIF-7 in the matrix of Pebax; hence the performance of Pebax membranes with moderate CO_2 affinity was less affected by the plasticization phenomenon. As can be seen in Fig. 10(d), a minor decline in ideal selectivity of all Il-Pebax 1657 membranes can be observed with pressure which agrees with the above explanation regarding the plasticization effect on membranes.

1-7. Mixed Gas Permeation Tests

The results of mixed gas permeation experiments performed on two separate binary gas mixture of (80 vol% CH_4 and 20 vol% CO_2) and (80 vol% N_2 and 20 vol% CO_2) are presented in Fig. 11.

As can be observed in this figure, the trend of changes in permeance and selectivity is the same when compared with pure gas tests results. However, except for ((IPZIF) sample, in mixed gas tests

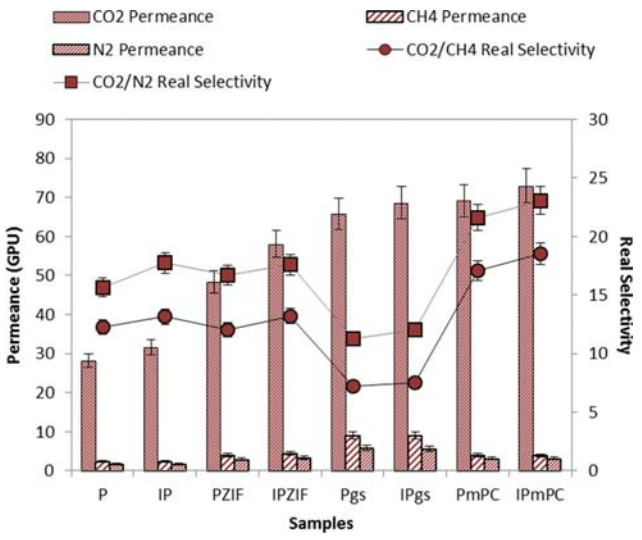

Fig. 11. The mixed gas permeance of CO_2, CH_4, and N_2 and real selectivity of CO_2/CH_4 and CO_2/N_2 for all synthesized membrane samples at the feed pressure of 4 bars and temperature of 20 °C.

generally, lower CO_2, CH_4, and N_2 permeance was measured. This happens due to the competing effect on permeation through modified and unmodified Pebax 1657 membranes. For the case of (IPZIF) sample, because this sample consists of large amounts of imidazole groups originating from DnBMCl in selective layer and ZIF-8 in the substrate, the sorption affinity for CO_2 in this sample was boosted and high amount of CO_2 was absorbed by (IPZIF). This elevated CO_2 sorption leads to an increase in CO_2 permeance of this sample [11]. It was approved that the gas molecules compete for the limited microvoid sorption sites in copolymers at low pressures of a mixed feed. This leads to a declining sorption capacity for gases and reduced flux of each penetrant [52,53]. The drop of sorption is more drastic for CH_4 and N_2 because PEO segments of Pebax 1657, DnBMCl, and ZIF-8 (for IPZIF) have a natural affinity for CO_2 sorption and not for CH_4 and N_2 [11]. Thus, despite the existence of competition in sorption, most of the sites have an affinity to be occupied by CO_2; hence the CO_2/CH_4 and CO_2/N_2 sorption selectivity enhanced in mixed gas conditions not only for (IPZIF) sample but also for all of the other synthesized samples compared with pure feed gas permeation results. Having the advantage of smaller kinetic diameter, the CO_2 molecules diffuse easier and faster in Pebax 1657 compared with larger molecules of CH_4 and N_2 [54]. Hence, the CO_2/CH_4 and CO_2/N_2 diffusivity selectivities are also higher in mixed gas conditions. The higher solubility selectivity and diffusivity selectivity in mixed gas conditions lead to higher selectivity of CO_2/CH_4 and CO_2/N_2 in mixed gas tests compared with pure gas experiments.

2. Results and Discussions of Modeling part

The calculated φ_v values at different temperatures based on measured densities are presented in Fig. 12.

As can be seen, the φ_v for macroporous PC support increases with the increase in temperature. This is because, with an increase in temperature, the mobility of polymeric chain in PC support increases and this leads to a decrease in bulk density of support, and consequently increases in its free and void volumes [55]. The increasing trend of change of φ_v with temperature is also observable for modified ZIF-8 support; the reason is that the temperature has a minor increasing effect on the pore volume of ZIF-8 [28]; hence with the increase in temperature the unoccupied volume in the bulk of ZIF-8 increases and this leads to increase in φ_v. This increase in

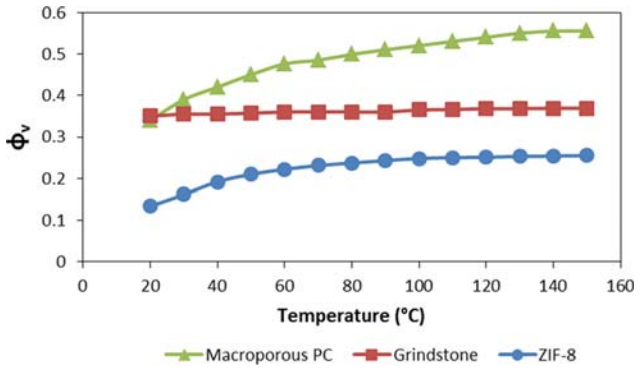

Fig. 12. The calculated void volume fractions for different types of fabricated substrates.

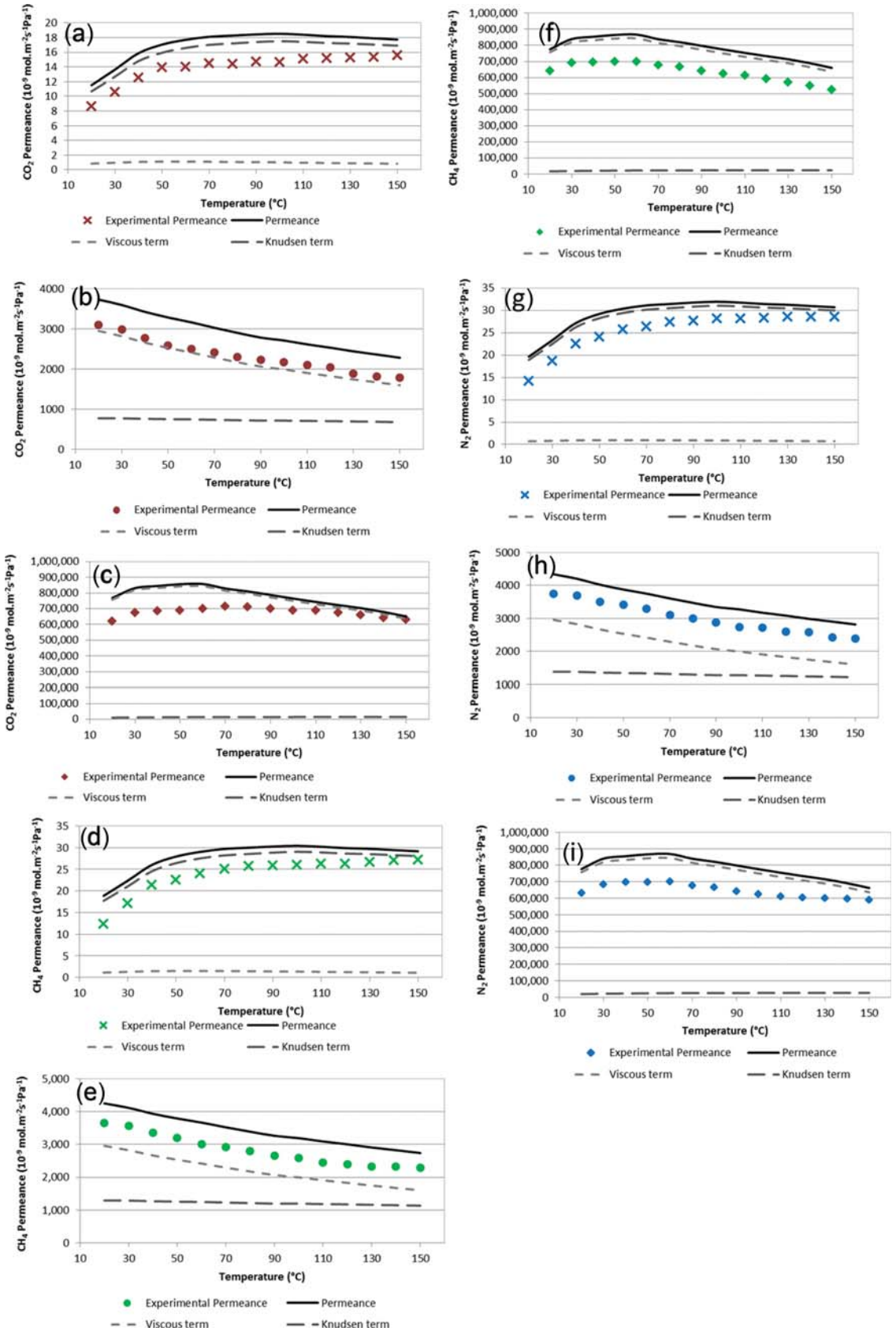

Fig. 13. The experimental and modeling values of gas permeance in (a) modified ZIF-8, (b) grindstone and (c) modified macroporous PC for CO_2, in (d) modified ZIF-8, (e) grindstone and (f) modified macroporous PC for CH_4 and in (g) modified ZIF-8, (h) grindstone and (i) modified macroporous PC for N_2 at different temperatures.

φ_v of ZIF-8 is more obvious at lower temperatures. This is because the percentage of temperature change at a lower temperature is higher than that at higher temperatures. There is no significant change in φ_v of grindstone with temperature. This is because the sandstone, the precursor of the grindstone, is unaffected by the rise in temperature, at least at the considered temperature range in this work [56]. Therefore, the porous nature of grindstone does not significantly change with the increase of temperature.

The results of CO_2, CH_4, and N_2 permeance along with the predicted permeance calculated based on viscous flow and Knudsen diffusion are presented in Fig. 13(a)-(i).

As can be seen in all subfigures of Fig. 13, the model without the introduction of the correction factor (α) overestimates the experimental permeance for all three considered gases in all three types of support. The reason is due to neglect of the tortuosity of the pore structure in DGM model for the porous substrates. The effect of ignoring tortuosity gradually vanishes with the rise in temperature and the predicted and experimental values of permeance converge for ZIF-8 and macroporous PC supports. The reason is related to the trend of change of φ_v with temperature and its effect on the tortuosity of support. As the φ_v increases, the relative void volume for gas diffusion increases in the support. This weakens the intensity of the effect of tortuosity on the diffusion of molecules and leads to the convergence of experimental and modeling values. For the case of grindstone support, because there is no significant change in φ_v with temperature, the differences between experimental data and model predictions remain almost constant with the rise in temperature. Another noteworthy point from this figure is that for each support with the change in the penetrating gas, the change in permeance is obvious except for macroporous PC. The reason is that the mean pore diameter for PC (890 nm) is extremely larger than the kinetic diameter of penetrating molecules; thus, the change in penetrating gas has a negligible effect on permeance through these pores. As can be seen in Fig. 13(a), (d), and (g), which are related to ZIF-8 support, the Knudsen diffusion mechanism is dominant in permeance of CO_2, CH_4, and N_2, and viscous flow has a minor effect on permeance of gases. This is due to the micropore regime of ZIF-8. In this range of pore size, the mean free path of molecules is comparable to the pore diameter; hence the Knudsen diffusion is the dominant gas transport mechanism. In Fig. 13(b), (e), and (h), which are related to grindstone substrate, both viscous flow, and Knudsen diffusion are effective in the overall gas transport mechanism. The mesoporosity of grindstone provides pore size that is slightly larger than the mean free path of gas molecules, but it is not large enough for fully viscous flow. Therefore, the permeance through the pores follows partial Knudsen diffusion and partial viscous flow. Fig. 13(c), (f), and (i), which are related to macroporous PC substrate, demonstrates that the viscous flow is the dominant mechanism defining gas transport through the macropores of PC support. The pore size in this type of support is significantly larger than the mean free path of molecules; therefore, the viscous flow has a dominating effect on the whole mechanism of gas transport through the pores and Knudsen diffusion has a negligible effect on the permeance of gases through macropores of PC. The relative share of different flow mechanisms in the overall mechanism of gas transport in three different support types is presented in Table S1 (see Supplementary file).

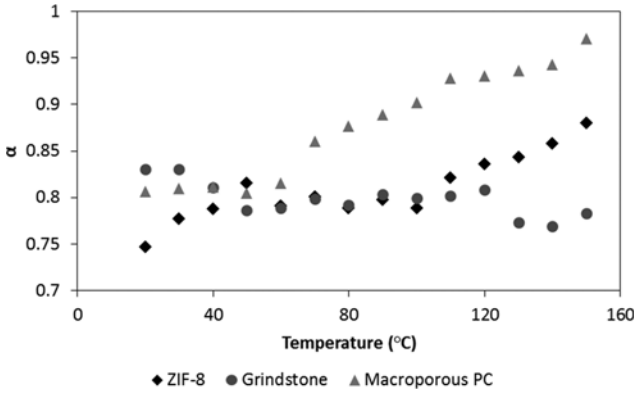

Fig. 14. The calculated values of the correction factor α for different types of substrates at different temperatures.

The changing trends of α values for CO_2, are presented in Fig. 14.

The α values for ZIF-8 have an increasing trend with temperature. The reason is that when the model predictions of CO_2 permeance decrease with temperature, the experimental data shows the same trend but with a margin [28]; therefore, the experimental data and model predictions tend to converge because the model does

Table 2. The predicted values of gas permeability based on Jia and Xu model

Sample	Gas	a_{1i}	b_{1i}	log(P)	P
P	CO_2	−2.138 [27]	0.626 [27]	1.892	77.930
IP				1.914	82.125
PZIF				1.926	84.306
IPZIF				1.949	88.843
Pgs				1.960	91.203
IPgs				1.971	93.625
PmPC				1.983	96.112
IPmPC				2.006	101.285
P	CH_4	3.445 [27]	0.687 [27]	0.977	9.488
IP				1.002	10.050
PZIF				1.015	10.343
IPZIF				1.040	10.956
Pgs				1.052	11.275
IPgs				1.065	11.604
PmPC				1.077	11.943
IPmPC				1.102	12.650
P	N_2	−3.512 [27]	0.659 [27]	0.729	5.361
IP				0.753	5.665
PZIF				0.765	5.824
IPZIF				0.789	6.154
Pgs				0.801	6.326
IPgs				0.813	6.503
PmPC				0.825	6.685
IPmPC				0.849	7.065

not account for pore size alteration with temperature. This regular trend cannot be seen for macroporous PC, probably because of the nonuniform change of its pore size. It also cannot be observed for grindstone, mainly because of its relatively stable pore size and structure, which is hardly affected by temperature change in the range investigated.

Table S2 shows the measured physical properties of membranes along with the calculated parameters related to these measured properties at 20 °C (see Supplementary file). Using FFV and v of membranes presented in Table S2, the cohesive energy density (E_{coh}) of 55000 for Pebax 1657, which was estimated from data for (E_{coh})s of PEO and PA6 based on Eq. (15) and the parameters of a_{1i} and b_{1i} of Jia and Xu, was used for prediction of the permeability of CO_2 in Pebax 1657 and TFC membranes at 20 °C (Table 2). As can be seen, the trend of change in predicted permeability of CO_2 follows the same trend of change in FFVs of membranes. This shows that even a slight increase in FFV results in a noticeable rise in the permeability of CO_2 in all synthesized membranes.

To acquire the correction factor (β) of FFV, a comparison between CO_2 experimental permeance and predictions of Jia and Xu

Table 3. The calculated effective thickness of TFC membranes based on the permeability of single-layer membranes at a feed pressure of 2 bars and a temperature of 20 °C

TFC membrane samples	Penetrating gas	Measured permeance (GPU)	Permeability of P and IP (Barrer)	Effective thickness (μm)
PZIF	CO_2	45.6	70	1.535
IPZIF		52.1	78	1.497
Pgs		57.8	70	1.211
IPgs		59.5	78	1.311
PmPC		65.0	70	1.077
IPmPC		69.0	78	1.130
PZIF	CH_4	2.2	3.5	1.591
IPZIF		2.3	3.5	1.500
Pgs		2.7	3.5	1.296
IPgs		2.7	3.5	1.286
PmPC		3.1	3.5	1.129
IPmPC		3.1	3.5	1.125
PZIF	N_2	3.8	5.7	1.500
IPZIF		4.0	5.9	1.475
Pgs		4.5	5.7	1.267
IPgs		4.6	5.9	1.283
PmPC		5.3	5.7	1.075
IPmPC		5.5	5.9	1.073

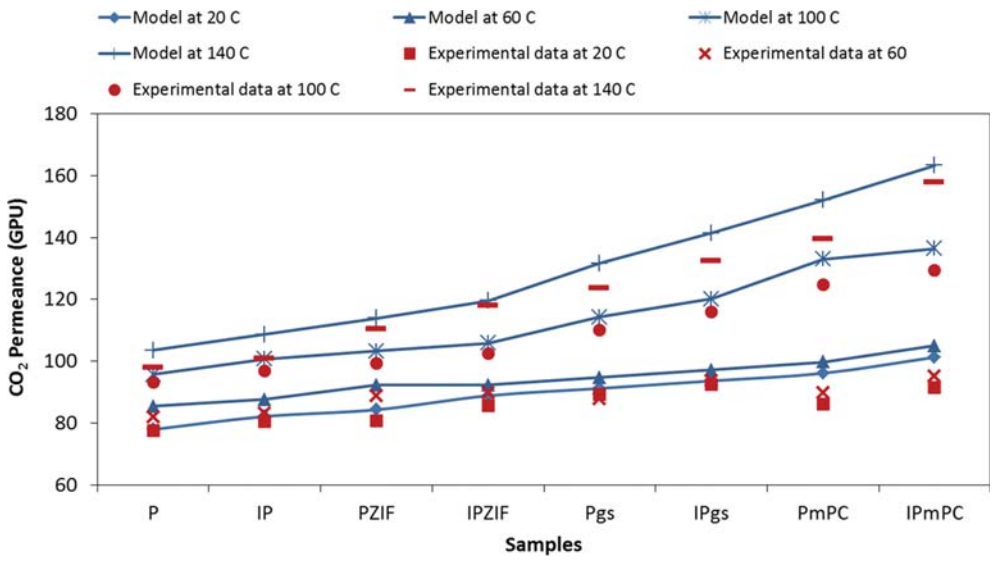

Fig. 15. The experimental permeance of CO_2 in all synthesized membranes together with the CO_2 permeance predicted by Jia and Xu model at different temperatures.

model was needed. Hence, the predicted permeability by Jia and Xu model were converted to permeance and the effective thicknesses of TFC membranes have been determined based on the permeability data presented in Table S3 (see Supplementary file) for Pebax 1657 and IL-Pebax 1657 single layer membranes. The detailed calculation procedure of effective thicknesses of TFCs can also be found in the Supplementary file.

Based on permeability presented in Table S3 for single-layer membranes, the effective thicknesses of selective layers of TFC membranes have been calculated and presented in Table 3.

All of the calculated effective thicknesses of TFCs have higher values than what is observed as presumed selective layers of TFCs in cross-sectional SEM micrographs of TFC membranes. This demonstrates that the synthesized substrates with different pore size regime and distribution show resistance against CO_2 flux through TFC membranes; hence their effect must be considered when predicting gas flux through the membranes.

Fig. 15 shows the experimental permeance of CO_2 through all synthesized membranes along with the CO_2 permeance predicted by Jia and Xu model at different temperatures.

The model values overestimate the experimentally measured CO_2 permeance for all of the synthesized membranes, especially at higher temperatures. The reason is most probably due to the overestimation of FFVs of membranes which are originating from the underestimation of membranes densities. In other words, the isolated pores and inaccessible voids, which were inevitably created in the porous substrate fabrication and membrane synthesis, reduce the density of membranes; however, they do not participate in gas transfer through the membranes [57,58], The fact that the overestimation of CO_2 permeance is more severe for TFC membranes with porous substrates supports the justification for underestimation of membrane densities. From the differences between model predictions and experimental data for CO_2 permeance the correction factor β, which accounts for the isolated pores and voids effect in membranes, has been determined and presented in Fig. 16.

Generally, the β values for TFCs on ZIF-8 substrates have higher values compared with those for TFC membranes on the grindstone or macroporous PC. This is most probably related to ordered open pore structure of ZIF-8 [59], which causes the measurement of density and calculation of FFV for TFCs on this substrate to be more accurate. Hence the model needs minor corrections and β values

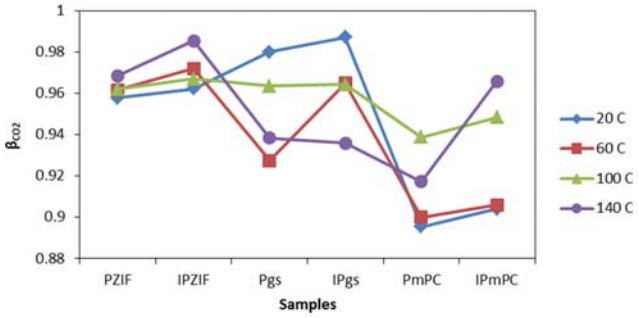

Fig. 16. The calculated correction factor β for CO_2 permeance in all synthesized membranes at different temperatures.

closer to unity. Although no regular trend of change can be observed for β with temperature in different TFC membrane samples, the β values for CO_2 have an almost similar trend of change with temperature as that the correction factor α for bare substrates experienced. It can be said that that there is a relationship between deviations of DGM and Jia and Xu model from the experimental permeance of CO_2 in substrates and TFC membranes. The reason is that the permeation in TFC membranes consists of solubility and diffusion in selective layer and diffusion in the porous substrate. Although the diffusion in TFCs is mainly controlled by diffusion in the selective layer, because of the similarities of selective layers of TFCs, the differentiating parameter in permeation in TFCs, ignoring the effect of IL, is the diffusion in substrates. Hence, it is anticipated that there must be a relationship between the correction factor of CO_2 permeance in TFC membranes and porous substrates.

The relationships between correction factors α and β of CO_2 permeance in TFCs on three different support types and at four different temperatures are presented in Fig. 17(a)-(c).

There is a linear relationship between correction factors α and β with noticeably large R-square. The linear dependency of β to α is presented in the charts. From these fitted line equations, it can be found that the dependency between β and α presented by these equations is only valid when α and β are large enough (e.g. >0.7). This means that to derive a relationship between correction factors, the predicting model for supports must be accurate and should be in relatively good agreement with experimental results.

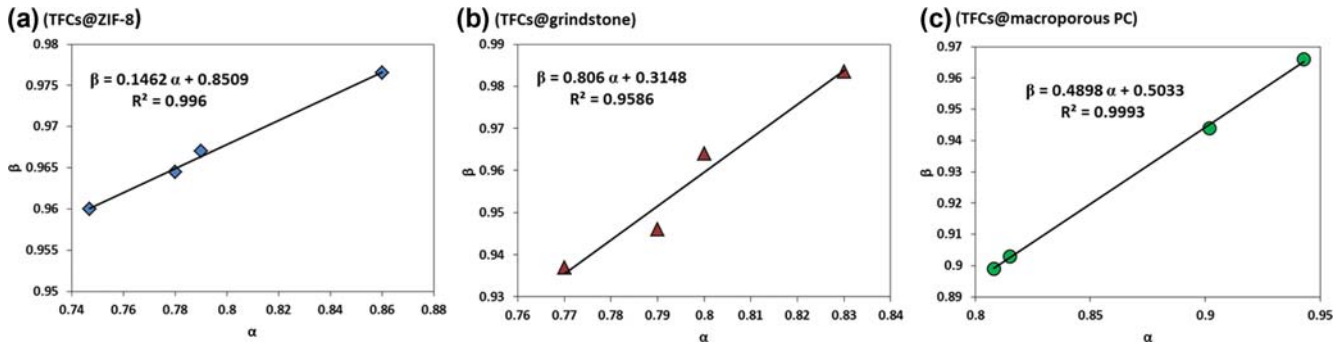

Fig. 17. The linear correlation between β and α obtained for CO_2 permeation in TFC membranes on (a) modified ZIF-8 support, (b) grindstone support and (c) modified macroporous PC support.

The obtained linear relationships between β and α for CO_2 was used to estimate the β values for CH_4 and N_2 permeance in TFC membranes based on α values obtained for CH_4 and N_2 permeance in three different supports. To do this, α values at different temperatures were extracted from subfigures (d), (e), and (f) of Fig. 13 for CH_4 and from subfigures (g), (h), and (i) of the same figure for N_2. These values were used as input for linear equations obtained in Fig. 17 for CO_2 to estimate the β values at different temperatures for CH_4 and N_2. The extracted α values and the calculated β values of CH_4 and N_2 for different synthesized TFC membranes at different temperatures are presented in Table S4 (see Supplementary file). The calculated β values were used to determine the predicted permeabilities of CH_4 and N_2 in TFC membranes. The results of the comparison between experimental and modeling permeabilities of CH_4 and N_2 for all TFCs at four different temperatures (20, 60, 100, and 140 °C) can be observed in Fig. 18(a)-(f).

As can be seen, with temperature increase, the permeability of CH_4 and N_2 increased, which was expected due to the increase in FFV of TFC membranes. In all subfigures of Fig. 18 the data points

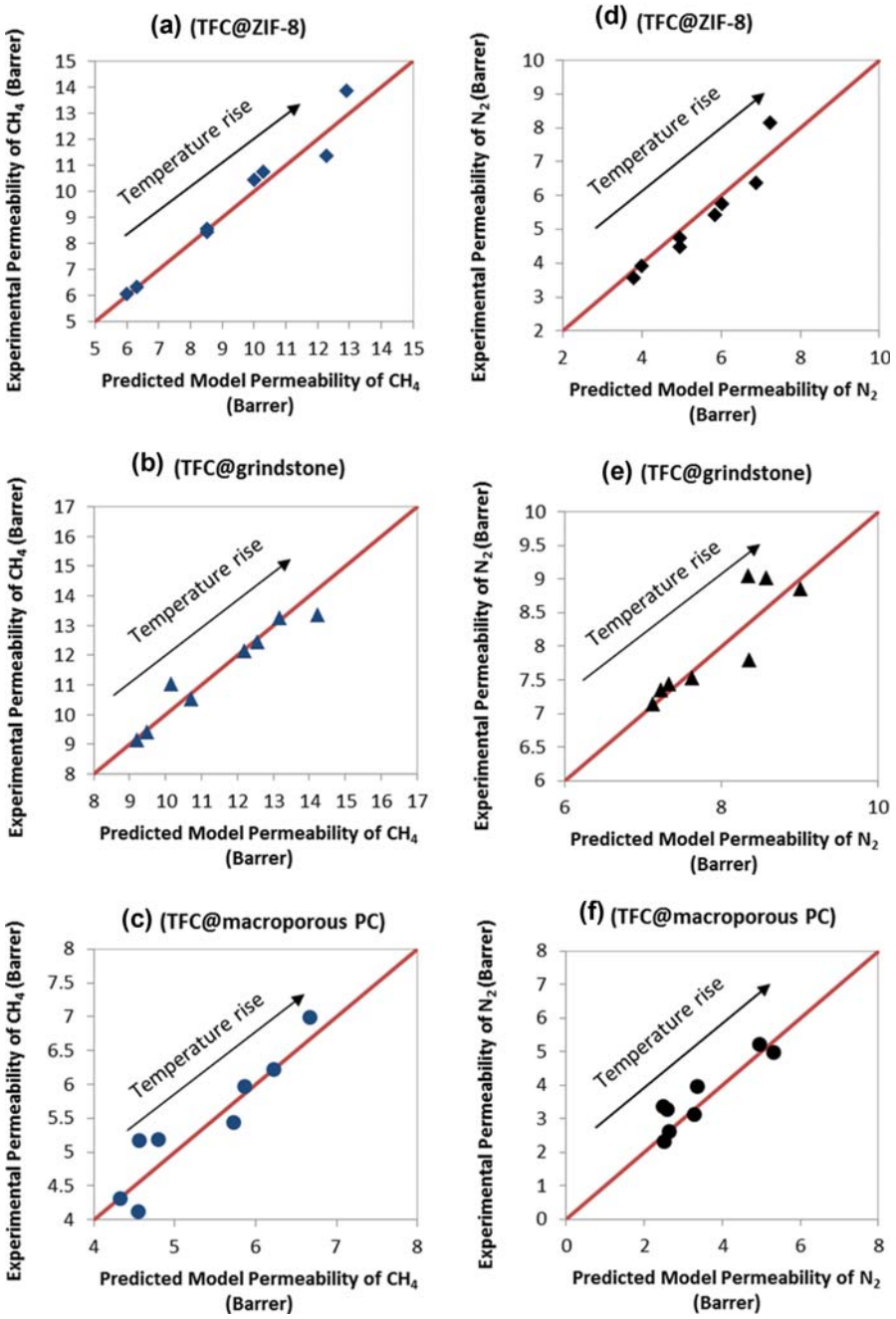

Fig. 18. The comparisons between experimental and model permeability values in TFC membranes on (a) modified ZIF-8 support, (b) grindstone support and (c) modified macroporous PC support for CH_4 and in TFC membranes on (d) modified ZIF-8 support, (e) grindstone support and (f) modified macroporous PC support for N_2 at four different temperatures.

Table 4. The %AARE and σ values of the modified Jia and Xu model (This work) in comparison with those of the original Jia and Xu model

Gas	PZIF & IPZIF				Pgs & IPgs				PmPC & IPmPC			
	Current work		Jia and Xu model		Current work		Jia and Xu model		Current work		Jia and Xu model	
	%AARE	σ	%AARE	σ	%AARE	σ	%AARE	σ	%AARE	σ	%AARE	σ
CH_4	3.13	4.14	4.46	4.54	2.48	3.67	3.44	3.79	5.21	6.54	10.51	7.57
N_2	7.22	6.40	9.71	6.85	3.27	4.19	4.39	5.38	10.91	12.39	12.72	13.49

are close to the line and there is a very good agreement between experimental data and model predictions. The reason for this good agreement is that all TFC membranes have the same selective layer material and method of fabrication; therefore, the most significant differences between them are related to their substrate type. Because α values are related to substrate type of TFC membranes and β values are related to FFVs calculated based on substrate type of TFCs, there must be a unique relationship between α and β regardless of penetrating gas in membranes as long as the calculated α and β values are not far from unity.

To compare the ability of our proposed model with Jia and Xu model in prediction of permeability of gases in single layers and TFC membranes, the average absolute relative error (%AARE) and standard deviation of errors (σ) have been calculated for both models based on the following equations [60]:

$$\%RE_i = \frac{P_i^{cal} - P_i^{exp}}{P_i^{exp}} \times 100 \tag{21}$$

$$\%ARE = \frac{100}{NDP} \sum_{i=1}^{NDP} RE_i \tag{22}$$

$$\%AARE = \frac{100}{NDP} \sum_{i=1}^{NDP} |RE_i| \tag{23}$$

$$\sigma = \sqrt{\frac{1}{NDP} \sum_{i=1}^{NDP} (\%RE_i - \%ARE_i)^2} \tag{24}$$

where NDP, RE, and ARE are abbreviations for numbers of data points, relative error, and average relative errors, respectively.

The values of %AARE and σ of models are presented for CH_4 and N_2 permeance through different TFCs in Table 4.

As can be seen in this table, the %AARE and σ of CH_4 and N_2 permeance for the proposed modified model are higher for all investigated TFC membranes compared with Jia and Xu model. This demonstrates not only that the modified model shows smaller overall deviations from experimental permeability values, but the deviations of these smaller deviations from average are also smaller for the modified model compared with Jia and Xu model. Thus, our predictions are closer to experimental values of permeability and the differences between model and experimental values are more similar to each other compared with predictions by original Jia and Xu model.

COMPARISON OF RESULTS WITH LITERATURE

The comparison of the CO_2/CH_4 and CO_2/N_2 separation performance of our synthesized IL-Pebax 1657 membranes with other IL-Pebax membranes synthesized and reported in the literature is presented in Fig. 19(a) and (b).

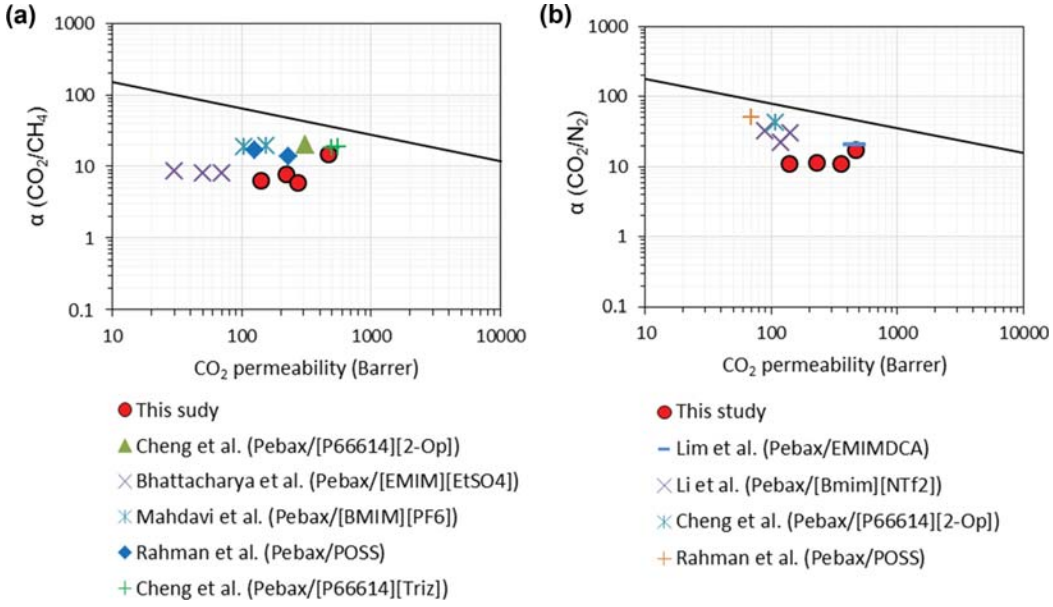

Fig. 19. The comparison of (a) CO_2/CH_4 and (b) CO_2/N_2 separation performance of IL-Pebax membranes of this work and IL-Pebax membranes synthesized by Cheng et al. [61,62], Bhattacharya et al. [63], Mahdavi et al. [64], Rahman et al. [65], Lim et al. [66] and Li et al. [67] with Robeson 2008 upper bond.

The CO_2 permeance of our synthesized IL-Pebax membranes, especially the sample fabricated on PC support, is superior to most of the compared cases. This is due to the negligible resistance of the macroporous support for gas permeation which was not observed in other investigated works. However, the CO_2/CH_4 and CO_2/N_2 selectivity of samples of this study are not very immersive compared with the other IL-Pebax membranes. This is because the concentration of IL in our final Pebax membrane structure was very low compared with other investigated cases. Because we used IL mainly for enhancement of compatibility of support and selective layer, the relatively low concentration of IL in synthesis solution of membranes has been applied in this work.

CONCLUSIONS

Innovative and high-performance ionic liquid modified Pebax 1657 TFC membranes were synthesized for CO_2/CH_4 and CO_2/N_2 separation. The novelty of the experimental part of this work was twofold: 1- Successful synthesis and utilization of an effective and rarely used ionic liquid for enhancement of compatibility between selective layer and support. 2- Successful synthesis of TFC membranes on three types of prepared and modified innovative substrates with unique pore structure to ensure the inclusion of all pore regimes in substrates used in the synthesis of TFC membranes for the study in modeling part of the work. In the experimental part of the study, XRD and FTIR analysis showed an improvement in the structural properties of ionic liquid-modified TFC membranes, which led to enhancement in their CO_2/CH_4 and CO_2/N_2 ideal and real selectivity. All IL-Pebax 1657 membranes showed thermal stability up to 320 °C. Significant increases in permeance of gases were observed at higher pressures with a minor decrease in selectivity. The remarkable CO_2 permeance of 470 GPU and CO_2/CH_4 and CO_2/N_2 selectivity of 14.2 and 16.4 were observed for the IL-Pebax 1657 membrane on macroporous PC support. In the modeling section of the work, porosity and tortuosity correction factors (α) were determined for different types of supports at different temperatures based on differences in experimental and dusty gas model of CO_2 permeation data. The correction factors of FFVs (β) were also determined by comparison of the experimental data with predictions of Jia and Xu model at different temperatures. The obtained linear relationships between α and β and the calculated α values for CH_4 and N_2 were used to determine β values for permeation through TFC membranes. Based on obtained values of AARE% and σ, the proposed modified Jia and Xu model showed great performance in the prediction of gas permeability in TFC membranes. In summary, this work provides a predictive relationship between correction factors of different types of substrates and those of TFC membranes; however, the experimental data for modeling this work was limited to permeation test results of the current work; hence, to derive a more generalized model in the future, more permeation data of TFC membranes have to be compared with the model predictions.

ACKNOWLEDGEMENTS

The Petroleum University of Technology (PUT) is acknowledged for providing materials and facilities for the experimental part of this work.

DECLARATION OF INTERESTS

The authors declare that they have no known financial interests or personal relationships that could have appeared to influence the work reported in this paper.

NOMENCLATURE

English Letters

A : effective area of membrane [cm^2]
Q_i : volumetric flowrate of permeated component i [$cm^3 \cdot s^{-1}$]
p_{fi} : partial pressure of component i at feed side [cmHg]
p_{pi} : partial pressure of component i at permeate side [cmHg]
W_{air} : the weight of sample in air [g]
W_{liq} : the weight of sample in determinant liquid [g]
FFV : fractional free volume
V_{Pebax} : total molar volume of Pebax 1657 [$cm^3 \cdot mol^{-1}$]
$V_{0,Pebax}$: volume occupied by polymer chains [$cm^3 \cdot mol^{-1}$)
M_{Pebax} : molar weight of a monomer of Pebax 1657 [$g \cdot mol^{-1}$]
$V_{W,Pebax}$: van der Waals volume of Pebax 1657 [$cm^3 \cdot mol^{-1}$]
V_{TFC} : specific volume of TFC membrane [$cm^3 \cdot g^{-1}$]
$v_{membrane}$: molar volume of membrane [$cm^3 \cdot mol^{-1}$]
d_p : mean pore diameter of substrate [cm]
J_v : volumetric flux of gas in viscous flow model [cm^3(STP)cm^{-2} s^{-1}]
J_K : volumetric flux of gas in Knudsen diffusion model [cm^3 (STP)$cm^{-2}s^{-1}$]
$\bar{p}$: mean feed and permeate pressure [cmHg]
M : molecular weight of penetrant [$g \cdot mol^{-1}$]
D_{Kn} : Knudsen diffusion coefficient
P : permeability coefficient of gases [(cm^3(STP)$\cdot cm \cdot cm^{-2}$ $cmHg^{-1}$ s^{-1}]
a_1 : first Jia and Xu coefficient for penetrating gas
b_1 : second Jia and Xu coefficient for penetrating gas
E_{coh} : cohesive energy density of polymers-gas [$J \cdot cm^{-3}$]
%RE : percent of relative error
%ARE : percent of average relative errors
%AARE : percent of average absolute relative errors
NDP : numbers of data points

Greek Letters

$\alpha_{A/B}$: Selectivity of gas A to gas B
ρ_{air} : the density of air [$g \cdot cm^{-3}$]
ρ_{liq} : the density of determinant liquid [$g \cdot cm^{-3}$]
ε : porous substrate porosity
τ : porous substrate tortuosity
μ : dynamic viscosity of gases [cmHg·s]
φ_v : void volume fraction
φ_{subs} : volume fraction of substrate in TFC membrane
ρ_{subs} : density of substrate [$g \cdot cm^{-3}$]
ω_{subs} : mass fraction of substrate in TFC membrane
ρ_{Pebax} : density of pure Pebax 1657 membrane [$g \cdot cm^{-3}$]
Π_i : permeance of penetrant i [cm^3(STP) s^{-1} cm^{-2} $cmHg^{-1}$]

Π_v : permeance of penetrant i based on viscous flow [cm^3(STP) s^{-1} cm^{-2} $cmHg^{-1}$]
Π_K : permeance of penetrant i based on Knudsen diffusion [cm^3 (STP) s^{-1} cm^{-2} $cmHg^{-1}$]
Π_{DGM} : permeance of penetrant i based on DGM [cm^3(STP) s^{-1} cm^{-2} $cmHg^{-1}$]
$\Pi_{Modified\ DGM}$: permeance of penetrant i based on modified DGM [cm^3(STP) s^{-1} cm^{-2} $cmHg^{-1}$]
δ : thickness of porous medium [cm]
δ_{skin} : thickness of skin layer [cm]
$\delta_{effective}$: effective thickness of membranes [cm]
α : correction factor of support non-ideality
β : correction factor of TFC non-ideality
γ : the surface tension of mercury [$J \cdot cm^{-2}$]
θ : contact angle [degree]
σ : standard deviation of errors
v_f : free volume of membrane [$cm^3 \cdot mol^{-1}$]

SUPPORTING INFORMATION

Additional information as noted in the text. This information is available via the Internet at http://www.springer.com/chemistry/journal/11814.

REFERENCES

1. S. Nesic, *Energy Fuels*, **26**, 4098 (2012).
2. B. Paschke and A. Kather, *Energy Procedia*, **23**, 207 (2012).
3. M. Wu, S. Wang and H. Liu, *J. Nat. Gas Sci. Eng.*, **16**, 81 (2007).
4. A. Jomekian, R. M. Behbahani, T. Mohammadi and A. Kargari, *J. Nat. Gas Sci. Eng.*, **31**, 562 (2016).
5. K. P. Shine, J. S. Fuglestvedt, K. Hailemariam and N. Stuber, *Clim. Change*, **68**, 281 (2005).
6. J. Gomes, S. Santos and J. Bordado, *Environ. Technol.*, **36**, 19 (2015).
7. C. Song, Q. Liu, S. Deng, H. Li and Y. Kitamura, *Renew. Sust. Energy Rev.*, **101**, 265 (2019).
8. A. Jomekian, R. M. Behbahani, T. Mohammadi and A. Kargari, *Korean J. Chem. Eng.*, **34**, 440 (2017).
9. W. Fam, J. Mansouri, H. Li and V. Chen, *J. Membr. Sci.*, **537**, 54 (2017).
10. J. Kim, Q. Fu, K. Xie, J. M. Scofield, S. E. Kentish and G. G. Qiao, *J. Membr. Sci.*, **515**, 54 (2016).
11. A. Jomekian, B. Bazooyar, R. M. Behbahani, T. Mohammadi and A. Kargari, *J. Membr. Sci.*, **524**, 652 (2017).
12. W. Fam, J. Mansouri, H. Li, J. Hou and V. Chen, *Ind. Eng. Chem. Res.*, **58**, 3304 (2019).
13. E. G. Estahbanati, M. Omidkhah and A. E. Amooghin, *ACS Appl. Mater. Interfaces*, **9**, 10094 (2017).
14. S. Meshkat, S. Kaliaguine and D. Rodrigue, *Sep. Purif. Technol.*, **200**, 177 (2018).
15. M. Mozafari, R. Abedini and A. Rahimpour, *J. Mater. Chem. A*, **6**, 12380 (2018).
16. G. Dong, J. Hou, J. Wang, Y. Zhang, V. Chen and J. Liu, *J. Membr. Sci.*, **520**, 860 (2016).
17. D. Zhao, J. Ren, Y. Wang, Y. Qiu, H. Li, K. Hua, X. Li, J. Ji and M. Deng, *J. Membr. Sci.*, **521**, 104 (2017).
18. P. Bernardo, J. C. Jansen, F. Bazzarelli, F. Tasselli, A. Fuoco, K. Friess, P. Izák, V. Jarmarová, M. Kačírková and G. Clarizia, *Sep. Purif. Technol.*, **97**, 73 (2012).
19. H. Rabiee, A. Ghadimi and T. Mohammadi, *J. Membr. Sci.*, **476**, 286 (2015).
20. A. Ghadimi, S. Norouzbahari, H. Lin, H. Rabiee and B. Sadatnia, *J. Membr. Sci.*, **563**, 643 (2018).
21. P. F. Lito, C. F. Zhou, A. S. Santiago, A. E. Rodrigues, J. Rocha, Z. Lin and C. M. Silva, *Chem. Eng. J.*, **165**, 395 (2010).
22. G. Z. Ramon, M. C. Wong and E. M. Hoek, *J. Membr. Sci.*, **415**, 298 (2012).
23. J. Wijmans and P. Hao, *J. Membr. Sci.*, **494**, 78 (2015).
24. O. M. Orogbemi, D. B. Ingham, M. S. Ismail, K. J. Hughes, L. Ma and M. Pourkashanian, *Int. J. Hydrogen Energy*, **41**, 21345 (2016).
25. O. M. Orogbemi, D. B. Ingham, M. S. Ismail, K. J. Hughes, L. Ma and M. Pourkashanian, *J. Energy Inst.*, **91**, 270 (2018).
26. L. Zhu, M. Yavari, W. Jia, E. P. Furlani and H. Lin, *Ind. Eng. Chem. Res.*, **56**, 351 (2016).
27. L. Jia and J. Xu, *Polym. J.*, **23**, 417 (1991).
28. A. Jomekian, R. Behbahani, T. Mohammadi and A. Kargari, *J. Solid State Chem.*, **235**, 212 (2016).
29. J. R. Caldwell and W. J. Jackson Jr., *J. Polym. Sci., Part C: Polym. Lett.*, **24**, 15 (1968).
30. M. Mubashir, Y. F. Yeong, K. K. Lau, T. L. Chew and J. Norwahyu, *Sep. Purif. Technol.*, **199**, 140 (2018).
31. J. Xiao and J. Wei, *Chem. Eng. Sci.*, **47**, 1123 (1992).
32. A. Fick, *The London, Edinburgh, & Dublin Philos. Mag. J. Sci.*, **10**, 30 (1855).
33. H. Yasuda and J. Tsai, *J. Appl. Polym. Sci.*, **18**, 805 (1974).
34. E. A. Mason and A. Malinauskas, *Gas transport in porous media: the dusty-gas model*, Elsevier Science Ltd., New York (1983).
35. I. Cabasso, K. Robert, E. Klein and J. Smith, *J. Appl. Polym. Sci.*, **21**, 1883 (1977).
36. D. Hua, Y. K. Ong, Y. Wang, T. Yang and T.-S. Chung, *J. Membr. Sci.*, **453**, 155 (2014).
37. Y. Shen and A. C. Lua, *Chem. Eng. J.*, **188**, 199 (2012).
38. A. Bondi, *J. Phys. Chem.*, **68**, 441 (1964).
39. A. Thran, G. Kroll and F. Faupel, *J. Polym. Sci., Part B: Polym. Phys.*, **37**, 3344 (1999).
40. H.-Y. Cho, J. Kim, S.-N. Kim and W.-S. Ahn, *Micropor. Mesopor. Mater.*, **169**, 180 (2013).
41. R. S. Murali, S. Sridhar, T. Sankarshana and Y. V. L. Ravikumar, *Ind. Eng. Chem. Res.*, **49**, 6530 (2010).
42. B. C. Smith, *Fundamentals of Fourier transform infrared spectroscopy*, CRC Press, Boca Raton (2011).
43. T. S. Chung, *Sep. Purif. Technol.*, **12**, 17 (1997).
44. I. Vankelecom, B. Moermans, G. Verschueren and P. Jacobs, *J. Membr. Sci.*, **158**, 289 (1999).
45. S. Couck, J. F. Denayer, G. V. Baron, T. Rémy, J. Gascon and F. Kapteijn, *J. Am. Chem. Soc.*, **131**, 6326 (2009).
46. I. Erucar and S. Keskin, *Ind. Eng. Chem. Res.*, **52**, 3462 (2013).
47. C. Cadena, J. L. Anthony, J. K. Shah, T. I. Morrow, J. F. Brennecke and E. J. Maginn, *J. Am. Chem. Soc.*, **126**, 5300 (2004).
48. A. Aquino, F. Bernard, J. Borges, L. Mafra, F. D. Vecchia, M. Vieira, R. Ligabue, M. Seferin, V. V. Chaban and E. Cabrita, *RSC Adv.*, **5**, 64220 (2015).

49. A. Car, C. Stropnik, W. Yave and K.-V. Peinemann, *Sep. Purif. Technol.*, **62**, 110 (2008).
50. J. M. Scofield, P. A. Gurr, J. Kim, Q. Fu, S. E. Kentish and G. G. Qiao, *Ind. Eng. Chem. Res.*, **55**, 8364 (2016).
51. P. Sharma, Y. J. Kim, M.-Z. Kim, S. F. Alam and C.-H. Cho, *Nanoscale Adv.*, **1**, 2633 (2019).
52. R. T. Chern, W. J. Koros, B. Yui, H. B. Hopfenberg and V. T. Stannett, *J. Polym. Sci., Part B: Polym. Phys.*, **22**, 1061 (1984).
53. R. T. Chern, W. J. Koros, E. S. Sanders and R. Yui, *J. Membr. Sci.*, **15**, 157 (1983).
54. J. H. Kim, S. Y. Ha and Y. M. Lee, *J. Membr. Sci.*, **190**, 179 (2001).
55. S. Hernández, F. Sket, J. M. Molina-Aldareguía, C. González and J. Llorca, *Compos. Sci. Technol.*, **71**, 1331 (2011).
56. M. Hajpál, *Fire Technol.*, **38**, 373 (2002).
57. K. Kaneko, *J. Membr. Sci.*, **96**, 59 (1994).
58. B. D. Zdravkov, J. J. Čermák, M. Šefara and J. Janků, *Cent. Eur. J. Chem.*, **5**, 385 (2007).
59. E. Barankova, N. Pradeep and K.-V. Peinemann, *Chem. Commun.*, **49**, 9419 (2013).
60. S. Hashemifard, A. Ismail and T. Matsuura, *J. Membr. Sci.*, **347**, 53 (2010).
61. J. Cheng, L. Hu, Y. Li, C. Ji, J. Zhou and K. Cen, *RSC Adv.*, **6**, 2055 (2016).
62. J. Cheng, L. Hu, Y. Li, J. Liu, J. Zhou and K. Cen, *Appl. Surf. Sci.*, **410**, 206 (2017).
63. M. Bhattacharya and M. K. Mandal, *J. Cleaner Prod.*, **156**, 174 (2017).
64. H. R. Mahdavi, N. Azizi, M. Arzani and T. Mohammadi, *J. Nat. Gas Sci. Eng.*, **46**, 275 (2017).
65. M. M. Rahman, V. Filiz, S. Shishatskiy, C. Abetz, S. Neumann, S. Bolmer, M. M. Khan and V. Abetz, *J. Membr. Sci.*, **437**, 286 (2013).
66. J. Y. Lim, J. K. Kim, C. S. Lee, J. M. Lee and J. H. Kim, *Chem. Eng. J.*, **322**, 254 (2017).
67. M. Li, X. Zhang, S. Zeng, H. Gao, J. Deng, Q. Yang and S. Zhang, *RSC Adv.*, **7**, 6422 (2017).

Supporting Information

Experimental and modeling study of CO_2 separation by modified Pebax 1657 TFC membranes

Abolfazl Jomekian*, Bahamin Bazooyar, and Reza Mosayebi Behbahani***,†**

*Esfarayen University of Technology, Esfarayen, North Khorasan, Iran
**Department of Design and Engineering, School of Creative Arts and Engineering, Staffordshire University, Stoke-on-Trent, ST4 2DE, United Kingdom
***Gas Engineering Department, Ahvaz Faculty of Petroleum Engineering, Petroleum University of Technology (PUT), Ahvaz, Iran
(*Received 4 April 2020 • Revised 26 May 2020 • Accepted 31 May 2020*)

Table S1. The relative shares of Knudsen diffusion and viscous flow mechanisms in DGM for different gases in different support types

Substrate	Penetrating gas	Knudsen diffusion share	Viscous flow share
ZIF-8	CO_2	94%	6%
	CH_4	95%	5%
	N_2	97%	3%
Grindstone	CO_2	25%	75%
	CH_4	36%	64%
	N_2	38%	62%
Macroporous PC	CO_2	2%	98%
	CH_4	3%	97%
	N_2	3%	97%

Table S2. The measured densities of membranes and substrates and related properties calculated based on them

Membrane samples	Measured density (cm^3/g)	$\varphi_{substrate}$	$\rho_{substrate}$ (cm^3/g)	$\omega_{substrate}$	FFV	v (cm^3/mol)
P	0.52±0.04	-	-	-	0.223	159.0
IP	0.52±0.05	-	-	-	0.224	159.2
PZIF	0.61±0.05	0.80	0.82±0.03	0.89	0.224	159.3
IPZIF	0.58±0.07	0.85	0.76±0.04	0.91	0.225	159.5
Pgs	1.16±0.08	0.95	1.61±0.02	0.98	0.226	159.6
IPgs	1.13±0.06	0.95	1.56±0.05	0.98	0.226	159.7
PmPC	0.38±0.04	0.75	0.45±0.01	0.78	0.227	159.8
IPmPC	0.35±0.05	0.69	0.40±0.02	0.71	0.228	160.0

Table S3. The permeability of modified and unmodified Pebax 1657 membrane at a feed pressure of 2 bars

Single-layer membranes	Penetrating gas	Permeance measured (GPU)	Effective thickness from SEM (μm)	Permeability (Barrer)
P	CO_2	27.8	2.52	70
IP		32.6	2.39	78
P	CH_4	1.39	2.52	3.5
IP		1.46	2.39	3.5
P	N_2	2.26	2.52	5.7
IP		2.47	2.39	5.9

Table S4. The obtained α and β of CO_2 at different temperatures for different TFC membranes

Temperature	PZIF & IPZIF		Pgs & IPgs		PmPC & IPmPC	
	α	β	α	β	α	β
40 °C	0.658	0.947	0.860	1.000	0.825	0.907
60 °C	0.827	0.972	0.821	0.977	0.808	0.899
100 °C	0.855	0.976	0.809	0.967	0.807	0.899
140 °C	0.918	0.985	0.822	0.977	0.798	0.894

EXPERIMENTAL DESIGN, MATERIALS, AND METHODS

As it is presented in table S3, First, the permeability of CO_2 in single layer Pebax 1657 and IL-Pebax 1657 was determined based on CO_2 permeances measured in pure gas permeation at a feed pressure of 2 bars. The effective thicknesses of single-layer membranes were determined using SEM micrographs from cross-sections of (P) and (IP) samples. Since in low feed pressures (e.g. 2 bars) the permeability of Pebax 1657 regardless of the thickness of the selective layer must remain constant, the calculated CO_2 permeabilities of single-layer membranes were considered the same as the CO_2 permeabilities of TFC membranes. Hence, based on the measured CO_2 permeances of Pebax 1657 and IL-Pebax 1657 single layer membranes which are presented in Table S3 and the assumed constant permeability of CO_2 in single layers and TFC membranes, the effective thicknesses of selective layers for TFC membranes have been calculated.